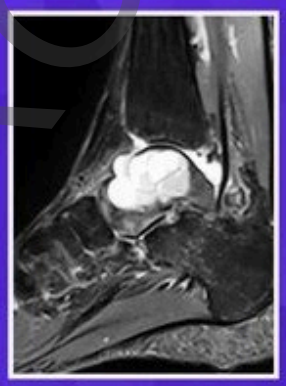
e www.ejaypee.com, for detailed information on radiology books, visit our website www.ejaypee.com, for detailed information on radiology books, visit our website www.ejaypee.com,

AIIMS-MAMC-PGI IMAGING SERIES

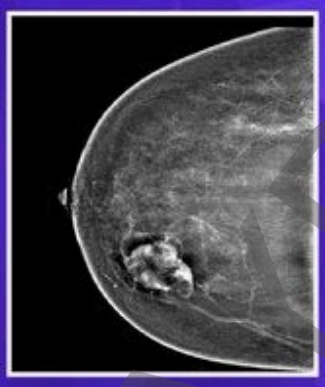
DIAGNOSTIC RADIOLOGY

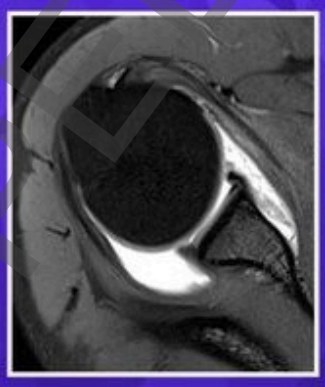
Musculoskeletal and Breast Imaging

Editors
Akshay Kumar Saxena
Raju Sharma
Alpana Manchanda









5th Edition

Associate Editors
Mahesh Prakash **Smriti Hari** **Swati Gupta**
Anindita Sinha **Surabhi Vyas** **Radhika Batra**

JAYPEE

JAYPEE BROTHERS

Contents

Section 1: Current Concepts and Intervention

1. **Current Concepts in Cross-Sectional Musculoskeletal Imaging** 3
   Shivanand Gamanagatti, Ankur Goyal, Raju Sharma
2. **Ultrasound in Musculoskeletal System** 24
   Madhurima Sharma, Anindita Sinha, Raghuraman Soundararajan, Mahesh Prakash
3. **Nuclear Medicine Imaging for Musculoskeletal Disorders** 45
   Rakesh Kumar, Bangkim Chandra Khangembam, Madhavi Tripathi
4. **Musculoskeletal Interventions** 61
   Kumble S Madhusudhan, Rajendra Kumar Behera

Section 2: Infections of Bones and Joints

5. **Tuberculosis of Bones and Joints** 77
   Gaurav Shanker Pradhan, Radhika Batra, Jyoti Kumar
6. **Nontubercular Bone and Joint Infections** 98
   Anindita Sinha, Manphool Singhal, Madhurima Sharma, Kushaljit Singh Sodhi
7. **Tuberculosis of the Spine** 117
   Rashmi Dixit, Gaurav Shanker Pradhan, Radhika Batra
8. **Nontubercular Infections of the Spine** 135
   Sameer Vyas, Chirag Kamal Ahuja, Ujjwal Gorsi

Section 3: Inflammatory, Metabolic and Degenerative Conditions

9. **Imaging in Rheumatological Disorders** 151
   Raghuraman Soundararajan, Mandeep Kang, Mahesh Prakash
10. **Degenerative Disease of the Spine** 176
    Jyoti Kumar, Anjali Prakash, Gaurav Shanker Pradhan
11. **Skeletal Disorders of Metabolic and Endocrine Origin** 195
    Alpana Manchanda, Jyoti Kumar, Swati Gupta, Sapna Singh
12. **Osteoporosis** 233
    Chirag Kamal Ahuja, Sameer Vyas, Vikas Bhatia, Ajay Kumar

JAYPEE BROTHERS

Section 4: Focal Bone Lesions and Bone Marrow Imaging

13. Diagnostic Approach to Focal Bone Lesions 253
Shivanand Gamanagatti, Sanchita Gupta, Raju Sharma

14. Benign Bone Tumors and Tumor-Like Conditions 270
Raghuraman Soundararajan, Mahesh Prakash, Anindita Sinha, Akshay Kumar Saxena

15. Malignant Bone Tumors 286
Radhika Batra, Rashmi Dixit, Sapna Singh, Swati Gupta

16. Imaging in Marrow Disorders: Benign and Malignant 327
Swati Gupta, Sapna Singh, Alpana Manchanda, Jyoti Kumar

Section 5: Magnetic Resonance Imaging of Joints

17. Magnetic Resonance Imaging of Shoulder and Temporomandibular Joints 369
Mahesh Prakash, Paramjeet Singh, Madhurima Sharma

18. Magnetic Resonance Imaging of the Elbow 397
Shivanand Gamanagatti, Ankur Goyal, Stanzin Spalkit

19. Magnetic Resonance Imaging of Wrist 429
Anindita Sinha, Madhurima Sharma, Harish Bhujade, Mahesh Prakash

20. Magnetic Resonance Imaging of the Hip and Pelvis 455
Anjali Prakash, Radhika Batra, Alpana Manchanda, Rashmi Dixit

21. Magnetic Resonance Imaging of the Knee 489
Sapna Singh, Anjali Prakash, Swati Gupta, Gaurav Shanker Pradhan

22. Magnetic Resonance Imaging of Ankle 541
Anindita Sinha, Madhurima Sharma, Mahesh Prakash

Section 6: Miscellaneous MSK-Trauma/Soft-Tissue/Nerve/Prosthetics Imaging

23. Imaging in Appendicular Trauma 565
Atin Kumar, Devasenathipathy Kandasamy, Amarinder Singh Malhi

24. Imaging of Soft-Tissue Tumors 581
Ankur Goyal, Priyanka Naranje, Ashu Seith Bhalla

25. Imaging of Peripheral Nerves 603
Mahesh Prakash, Harish Bhujade, Anindita Sinha

26. Imaging of the Brachial and Lumbosacral Plexus 623
Mahesh Prakash, Raghuraman Soundararajan, Madhurima Sharma, Anindita Sinha

27. Imaging in Prosthetic Joints 646
Ankur Goyal, Shivanand Gamanagatti, Stanzin Spalkit

JAYPEE BROTHERS

Section 7: Breast Imaging and Interventions

28. A Systematic Approach to Imaging of Breast Lesions **667**
Smriti Hari, Surabhi Vyas, Manisha Jana

29. Breast Imaging Reporting and Data System and Recent Updates **687**
Surabhi Vyas, Smriti Hari, Sanchita Gupta

30. Benign and Malignant Lesions of the Breast **711**
Smriti Hari, Smita Manchanda, Ekta Dhamija

31. Breast Interventions **742**
Surabhi Vyas, Smriti Hari, Krithika Rangarajan

32. Advances in Breast Imaging **763**
Tulika Singh, Veenu Singla, Uma Debi

33. Male Breast Imaging **782**
Veenu Singla, Tulika Singh, Nidhi Prabhakar, Raghuraman Soundararajan

34. Breast Cancer Screening **794**
Anjali Prakash, Alpana Manchanda, Rashmi Dixit

Index **805**

JAYPEE BROTHERS

CHAPTER 19

Magnetic Resonance Imaging of Wrist

Anindita Sinha, Madhurima Sharma, Harish Bhujade, Mahesh Prakash

JAYPEE BROTHERS

INTRODUCTION

Wrist is composed of complex joint formed by small bones, ligaments, tendons, and cartilage. Magnetic resonance imaging (MRI) is an important diagnostic tool in the evaluation of common wrist disorders and ligamentous injuries. For accurate diagnosis of various pathologies of wrist, it is important to know detailed anatomy of wrist.

BONES AND JOINTS

Wrist is formed by distal radius and ulna, eight carpal bones, and bases of metacarpals. The proximal row is formed by scaphoid, lunate, triquetrum, and pisiform; the distal row is formed by trapezium, trapezoid, capitate, and hamate (from lateral to medial). The distal ends of radius and ulna form the distal radioulnar joint (DRUJ). The radius has a triangular articular surface for the scaphoid and a quadrilateral articular surface for the lunate at its distal end to form the radiocarpal joint.

The two rows of carpal bones form *Gilula's arc*, which comprised of Arc I along the proximal surfaces of proximal carpal bones (scaphoid, lunate, and triquetral), Arc II along the distal surfaces of these proximal carpal bones, and Arc III along the proximal surfaces of capitate and hamate **(Fig. 1)**.[1]

Ulnar Variance

Ulnar variance is the difference in lengths of articular surfaces of distal ends of radius and ulna.[2] This can be neutral when both articular surfaces are at the same level, negative (ulnar articular surface > 2 mm proximal to the radial articular surface), and positive (ulnar articular surface > 2 mm distal to radial articular surface) **(Figs. 2A to C)**.

Ligaments of Wrist

For convenience, the wrist ligaments are grouped into intrinsic ligaments, extrinsic ligaments, and ligaments of thumb.

Intrinsic ligaments attach only to carpal bones and include scapholunate ligament, lunotriquetral ligament, and triangular fibrocartilage complex (TFCC) **(Fig. 3)**.

Extrinsic ligaments attach to other structures besides carpal bones. These are further divided into volar extrinsic and dorsal extrinsic ligaments:

- *Volar extrinsic ligaments* consist of volar radioscaphocapitate, volar radiotriquetral, volar ulnolunate, volar ulnotriquetral, and volar radioulnar ligaments.

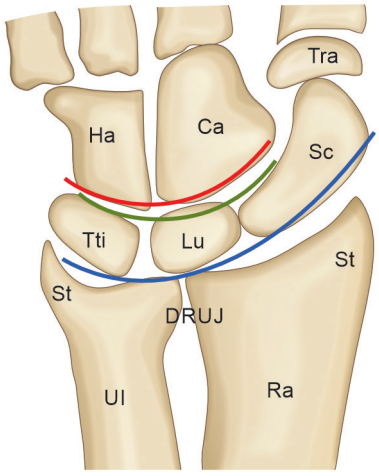
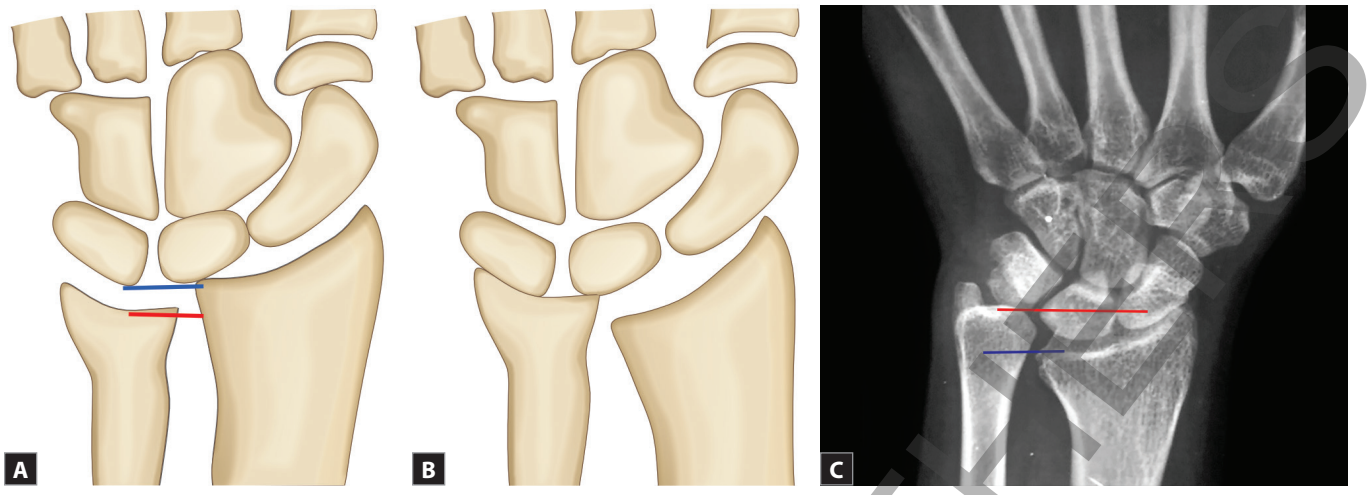


FIG. 1: Bones of the wrist with carpal bones forming the three arcs of Gilula. Proximal row (blue) is formed by the proximal articulating surfaces of scaphoid (Sc), lunate (Lu), and triquetral (Tri). The II arc (green) is formed by the distal articulating surfaces of the proximal carpal bones. The III arc (red) is formed by the proximal articulating surface of capitate (Ca) and hamate (Ha). The radius (Ra), ulna (Ul), and styloid processes (St) and the distal radioulnar joint (DRUJ) are shown. Note the neutral ulnar variance.



FIGS. 2A TO C: Ulnar variance. Ulnar variance is measured as the distance between two lines, one drawn tangential to the lunate fossa of radius (blue line) and another drawn tangential to the ulnar articular surface of ulna. (A) Negative ulnar variance with a short ulna; (B) Positive ulnar variance with ulna longer than the distal radius; (C) Radiograph of the wrist showing positive ulnar variance.

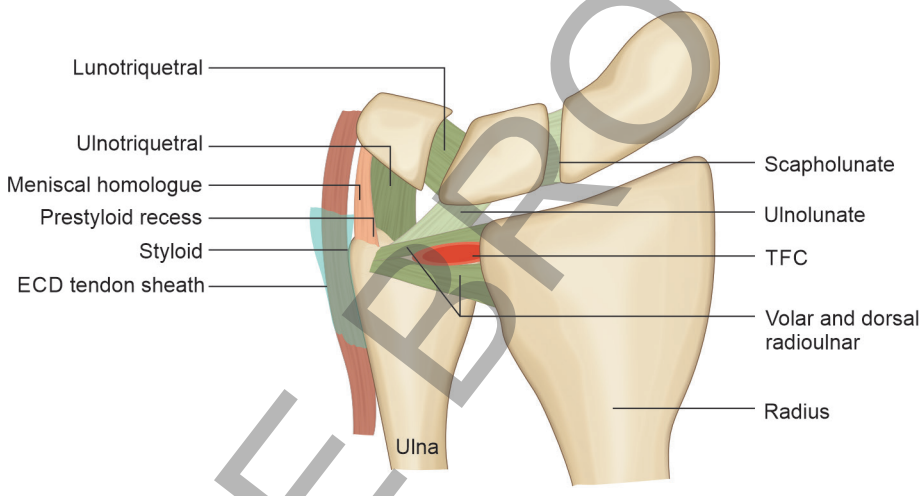


FIG. 3: Components of triangular fibrocartilage complex. The triangular articular disc (TFC disc proper), the volar, and dorsal radioulnar ligaments, the ulnolunate ligament, the ulnotriquetral ligament, the ulnar collateral ligament, the meniscus homologue, and part of the sheath of the extensor carpi ulnaris tendon. The scapholunate and lunotriquetral ligaments are also shown.
(ECU: extensor carpi ulnaris; TFC: triangular fibrocartilage).

- *Dorsal extrinsic ligaments* consist of dorsal intercarpal, dorsal radiotriquetral, and dorsal radioulnar ligaments.

Scapholunate Ligament (Fig. 3)

Scapholunate ligament is a U-shaped ligament and has three components: Volar, dorsal, and interosseous.[3] The volar component, which courses obliquely, is thinner (1 mm in thickness) and weaker. The dorsal component is the thickest component (3 mm). The volar and dorsal components are best seen on axial images, appearing as band-like structures, the dorsal showing homogeneous-signal intensity and the volar showing heterogeneous-signal intensity. The interosseous component is best viewed on coronal sections. It appears band-like at its dorsal aspect, triangular at its central aspect, and trapezoidal at its volar aspect.

Lunotriquetral Ligament (Fig. 3)

Lunotriquetral ligament appears V-shaped and has volar, dorsal, and proximal components. The dorsal component is important for carpal stability and resistance to rotation.[3] The volar and dorsal components appear band-like on axial images.

Triangular Fibrocartilage Complex (Fig. 3)

Triangular fibrocartilage complex lies between the distal end of ulna and proximal carpal bones (lunate

JAYPEE BROTHERS

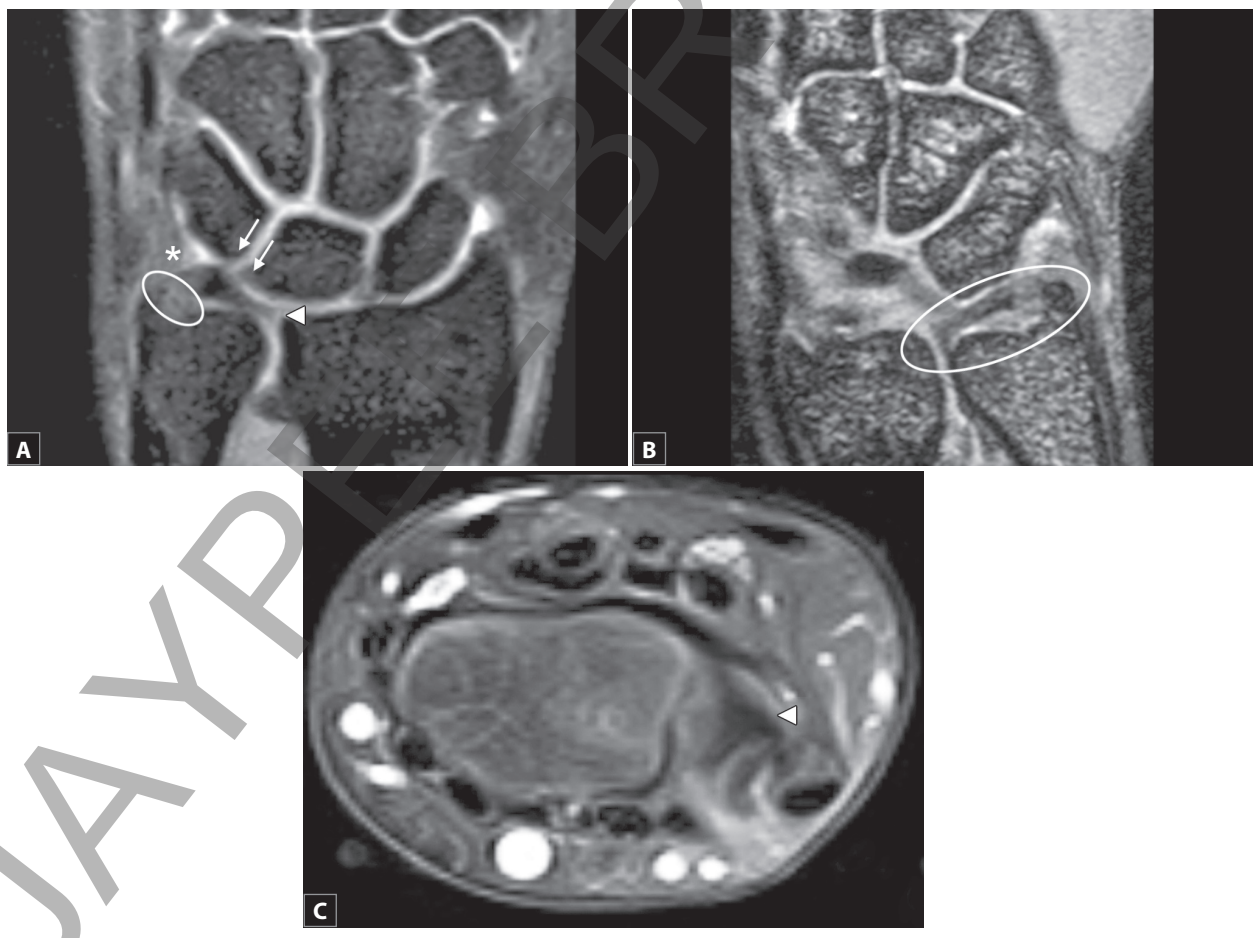
and triquetral). It consists of a triangular articular disc [triangular fibrocartilage (TFC) disc proper], dorsal radioulnar ligament, volar radioulnar ligament, ulnolunate ligament, ulnotriquetral ligament, ulnar collateral ligament, meniscus homologue, and part of the sheath of the extensor carpi ulnaris (ECU) tendon. The appearance of TFCC varies with ulnar variance. It is thicker and short with negative ulnar variance and thin and stretched with positive ulnar variance.

Triangular fibrocartilage disc appears as an asymmetric bowtie structure, which is best seen on coronal sections as a low-signal intensity structure on all pulse sequences. The triangular ligament has two bands, which attach the disc proper to the tip and fovea of the styloid process of ulna **(Figs. 4A to C)**. The vascularized tissue between the two bands is called the ligamentum subcruentum. TFC is supplied by the palmar and dorsal branches of the anterior interosseous artery and branch of the ulnar artery. The central and radial part of TFC is avascular while the periphery is vascularized. The tears of the vascularized part of TFC get healed while those of the central and radial part do not heal.[3]

The meniscal homologue appears as a triangular fat intensity structure between the ulnar styloid and triquetrum. It joins the ECU tendon sheath and joint capsule to form a ligamentous stabilizer.[4]

The radioulnar ligaments (dorsal and volar) are the main stabilizers of the wrist and DRUJ. It has superficial and deep fibers, both arising from the ulnar side of the distal radius at the sigmoid notch. The deep fibers insert on the fovea of the styloid process of ulna and are most important for joint stability, and the superficial fibers attach to the tip of the ulnar styloid.[5]

The volar ulnolunate ligament arises from the volar radioulnar ligament. It attaches distally to the lunate, parallel to the long axis of the wrist and forearm. Some of its fibers also attach to the lunotriquetral ligament. The volar ulnotriquetral ligament also arises at the volar radioulnar ligament, medial to the volar ulnolunate ligament. This ligament then broadens and attaches on the triquetrum. Both these volar ligaments can be best seen on coronal images. The volar radioscaphocapitate ligament arises from the radial styloid and courses distally and medially to the capitate. Few of its fibers attach to the waist of scaphoid.



FIGS. 4A TO C: Normal TFCC-hyperintensity on coronal T2W fat-saturated image (A) at radial (arrowhead) and ulnar (oval) attachment sites. The central disc is biconcave and hypointense. Meniscal homologue (asterisk), ulnolunate, and ulnotriquetral ligaments (small arrows) are seen; (B) T2*W coronal image—the ulnar and dorsal radioulnar ligaments (oval) have flat superior and inferior margins; (C) The triangular fibrocartilage may be visualized on axial images as a dark hypointense triangle (arrowhead).
(TFCC: triangular fibrocartilage complex)

JAYPEE BROTHERS

The volar radiolunate ligament also arises from the radial styloid, adjacent to the radioscaphocapitate ligament origin. The volar radiolunate ligament extends obliquely to attach on the lunate.

The dorsal radiotriquetral ligament arises from the dorsal styloid process of radius and attaches to the dorsal tubercle of the triquetrum. It courses in an oblique fashion, attaching and crossing the medial aspect of the lunate. The dorsal intercarpal ligament spans from the dorsal tubercle of the triquetrum to the dorsal groove of the scaphoid. The dorsal radiotriquetral and dorsal intercarpal ligaments are best evaluated on coronal images.[3]

Extensor Compartment (Fig. 5)

The extensor retinaculum stretches between the ulnar styloid process, the medial margin of pisiform and triquetrum, and the lateral radius margin. From the radial to the ulnar side, the extensor tendons are arranged under the extensor retinaculum into six extensor compartments. The extensor tendons are best evaluated on axial images.

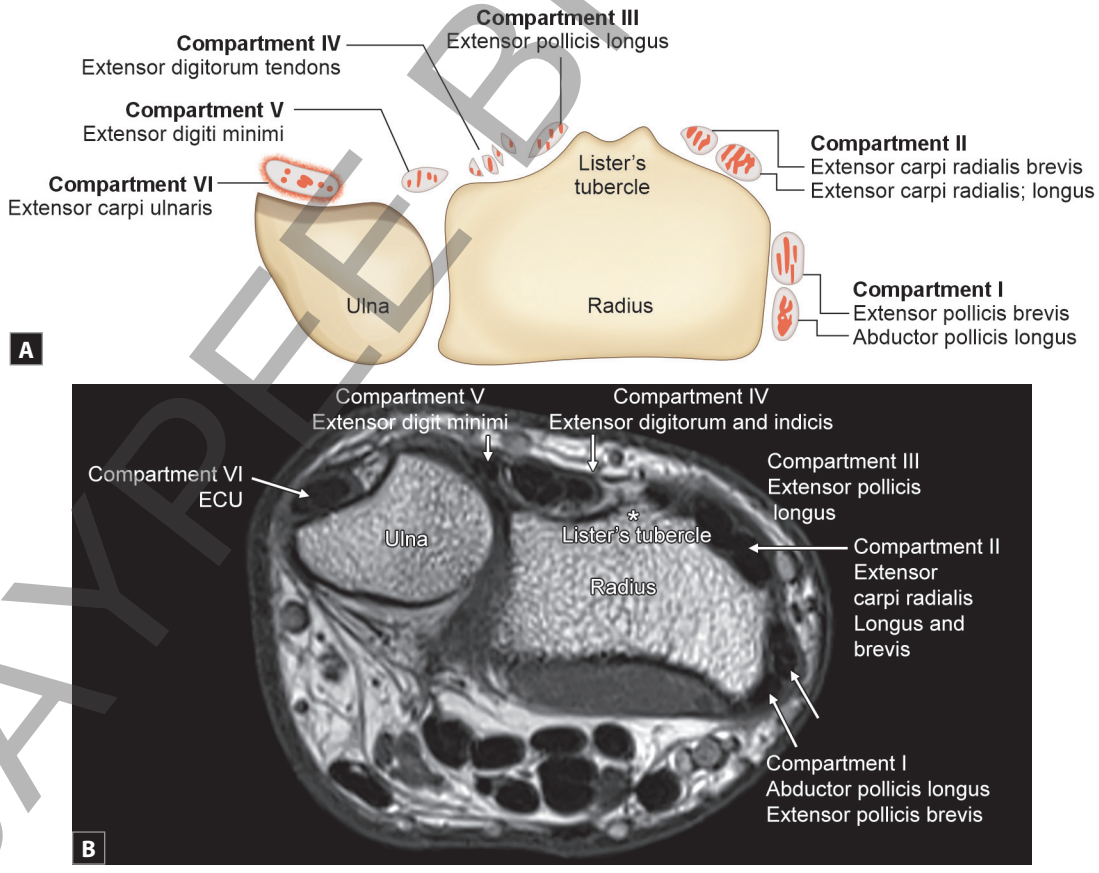
- *Compartment I*: Abductor pollicis longus (APL) and extensor pollicis brevis (EPB) tendons
- *Compartment II*: Extensor carpi radialis longus and brevis tendons
- *Compartment III*: Extensor pollicis longus (EPL) tendon
- *Compartment IV*: Extensor digitorum and indicis tendons
- *Compartment V*: Extensor digiti minimi tendon
- *Compartment VI*: Extensor carpi ulnaris tendon

Flexor Compartment (Figs. 6A to C)

A total of nine tendons traverse the carpal tunnel passing under the flexor retinaculum, which includes the four deep flexor digitorum profundus (FDP) tendons, the four superficial flexor digitorum superficialis (FDS) tendons, and the single flexor pollicis longus (FPL) tendon.

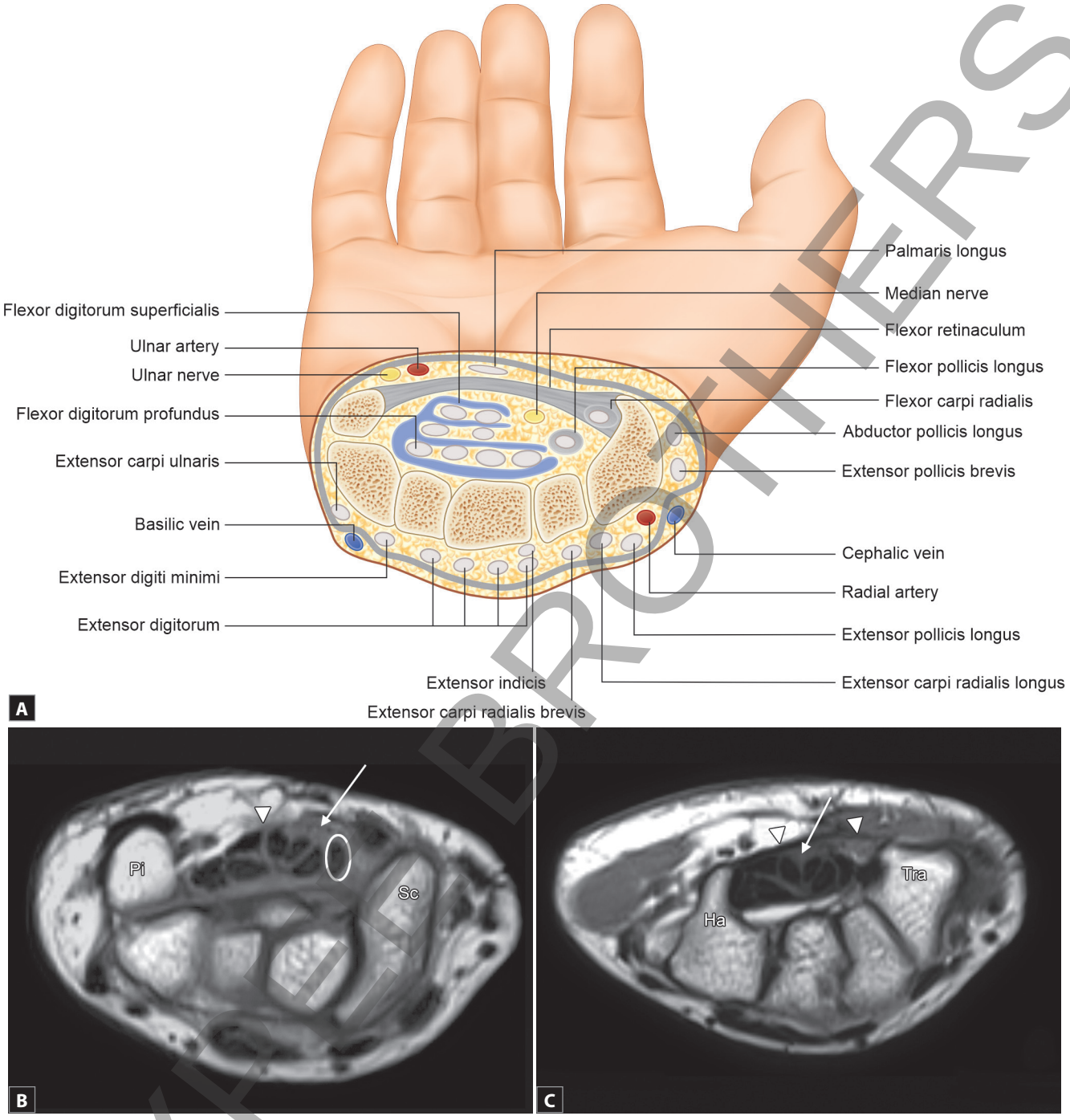
Carpal Tunnel (Figs. 6A to C)

Carpal tunnel is formed on the volar aspect of the wrist joint by the flexor retinaculum (transverse carpal ligament) forming the fibrous roof. The floor is formed by the carpal bones. The flexor retinaculum attaches to the scaphoid proximally on the radial side and tubercle of trapezium distally. The retinaculum attaches to the pisiform proximally and hook of hamate distally on the ulnar side.



FIGS. 5A AND B: (A) From the radial to the ulnar side, the extensor tendons are arranged under the extensor retinaculum into six extensor compartments. Lister's tubercle (*) is a landmark dividing compartments II and III. (B) Axial T1W image of the wrist at the level of the distal radioulnar joint shows the six extensor compartments.

JAYPEE BROTHERS



FIGS. 6A TO C: (A) Carpal tunnel and Guyon's canal. Normal magnetic resonance (MR) anatomy of the carpal tunnel. Axial T1W MR images (B) at the level of pisiform and (C) at the level of hook of hamate showing the fibro-osseous carpal tunnel bounded by the carpal bones posteriorly, by the pisiform and hook of hamate on the ulnar side, and the scaphoid and tubercle of trapezium on the radial side. Superiorly, the hypointense linear flat flexor retinaculum (arrowheads) forms the roof of the carpal tunnel. The hypointense flexor digitorum superficialis and profundus tendons and the fasciculated speckled median nerve (arrow) are seen traversing the tunnel. The tendon of flexor pollicis longus (oval) is deep to the median nerve.
(Ha: hook of hamate; Pi: pisiform; Sc: tubercle of scaphoid; Tra: trapezium)

The carpal tunnel contains the median nerve, the flexor tendons (four each of FDS and FDP surrounded by a single synovial sheath), and the FPL in a separate synovial sheath.

Guyon's Canal

- Guyon's canal is a small fibro-osseous space on the ulnar side of the volar aspect of wrist.
- *Medial border*: Pisiform bone, flexor carpi ulnaris tendon
- *Lateral border*: Hook of the hamate
- *Roof*: Palmar carpal ligament
- *Floor*: transverse carpal ligament (flexor retinaculum), pisohamate and pisometacarpal ligaments, FDP. Opponens digiti minimi muscle is sometimes present and can cause compression symptoms

JAYPEE BROTHERS

- *Contents*: Ulnar nerve, ulnar artery, and venae commitans. The ulnar nerve branches into superficial (sensory) and deep (motor) branches.

IMAGING TECHNIQUE OF WRIST

Magnetic Resonance Imaging

A 3 Tesla scanner is preferable for high-resolution imaging of the small intrinsic ligamentous structures of the wrist.[6]

Positioning

Careful positioning is essential to minimize artifacts and avoid misinterpretation of ligament and tendon abnormalities. Patient coaching and reassurance, wrist stabilization with padding or foam, straightening of the fingers, and avoidance of wrist rotation help obtain diagnostic-quality images.[7]

Patients can be placed in prone position with arms outstretched above the level of head (Superman position). However, this position is difficult in obese patients and patients with shoulder or respiratory problems. Patients can also be supine in reverse Superman position with the arm stretched above the head and dorsum of the hand on the table.[7] Patients unable to stay in this position can stay in supine position with hand beside the body with the hand midway between pronation and supination at 90° to the table.[7] In this position, a single hand and wrist can be imaged by a phased array coil; however, image quality including fat suppression may be suboptimal due to distance of wrist and hand from the isocenter of the magnet. Additional manual shimming and use of fat suppression techniques such as IDEAL (iterative decomposition of water and fat with echo asymmetry and least-squares estimation) can overcome these problems.[6] Patients can also be placed with a gap between the hand and body with additional saturation bands or phase oversampling to avoid wrap around from the body.[7]

Coil

A dedicated 8–16-channel wrist (surface) coil is ideal for wrist. Small flex or loop coils can be used for cases where only a small field of view is needed for imaging of a dedicated structure. These coils can be closely wrapped around the anatomical part to be imaged.

The suggested protocol is given in **Table 1**.

Sequences are given in **Table 2**.

The three-dimensional fast spin-echo (3D FSE) isotropic sequences are better than gradient recalled echo (GRE) for cartilage, ligament, and osseous evaluation. These techniques can be quickened by parallel imaging, driven equilibrium techniques, compressed SENSE, or variable flip angles of the radiofrequency (RF) refocusing pulse. [For example, SPACE (Sampling Perfection with Application optimized Contrasts using different flip angle Evolution), CUBE, and VISTA (volume isotropic turbo spin-echo acquisition) are techniques in various scanners.][8]

TABLE 1: MRI protocol planning routine imaging of the wrist.

Field of view	8–10 cm
Matrix	416 × 192, 224 × 224 (for 3D sequences)
Slice thickness	2–2.5 mm with no interslice gap
Imaging plane	Axial scout-to-plan coronal (coronal should be the first sequence)
Coronal	Coronal-parallel to ulnar and radial styloid process [coverage from bases of metacarpals to distal radioulnar joint (DRUJ)]
Axial	Coronal scout-to-plan axial
	Axial images should include carpometacarpal joints and DRUJ
Sagittal	Use axial images to plan
	Sagittal images should be perpendicular to volar tips of the scaphoid tubercle and pisiform

TABLE 2: MRI sequences.

Coronal	• T2 FS • T1 • PD FS* (keep TE at 40, not less for PD sequences)
Axial	• T2 FS • T1
Sagittal	PD FS
Coronal 3D isotropic sequence7	T2* GRE, 3D volumetric FSE PD FS turbo spin echo with <1 mm slice thickness

*Keep TE at 40, not less for PD sequences.

(FS: fat-saturated; FSE: fast spin-echo; GRE: gradient recalled-echo; PD: proton density; TE: echo time)

Cartilage Imaging

Cartilage imaging has the potential of early detection of degenerative changes and tears of TFCC and articular cartilage of carpal bones. Preliminary studies have suggested changes in T1rho (T1ρ) and T2 relaxation times in torn ligaments and in degenerative and inflammatory conditions, as well as changes in response to different medications in inflammatory arthritis.[9,10]

Magnetic Resonance Arthrography of Wrist

Magnetic resonance arthrography of wrist can be single-compartmental (most commonly radiocarpal), two-compartmental, or rarely three-compartmental

JAYPEE BROTHERS

(radiocarpal, DRUJ, and midcarpal) arthrography. The fluoroscopic guidance is used for injections into the joint. The dorsal approach is commonly used for radiocarpal injections. The lateral approach can be used for radiocarpal injections.[11] The radiocarpal joint is visualized, and skin surface is marked at the level of the midscaphoid. Local anesthesia is given with a 22–26 gauge, hypodermic needle on the dorsum of the wrist. 3–5 mL of 1:1 contrast media (diluted iodinated contrast and gadolinium) is injected till the resistance is felt under fluoroscopic/cine guidance after advancing the needle into the radiocarpal joint.

The dorsal approach can also be used for midcarpal and DRUJ injections. For midcarpal injections, the needle is advanced into the central part of the junction of the hamate, lunate, capitate, and triquetrum. For DRUJ injection, the needle extends to the radial aspect of the ulnar head.[12]

Indications for MR arthrography include peripheral TFC tears, undersurface TFCC tears as well as for evaluation of the postoperative TFCC where the injection site should be DRUJ. MR arthrography also increases diagnostic confidence in detecting tears of scapholunate and lunotriquetral ligaments.[13]

The contraindications for wrist injections include local skin infections. Pain and swelling may be seen after the injections, which is likely due to overdistension of joints.

Magnetic resonance arthrography is performed after the injections on 1.5 T or higher tesla machine. The position of patient is like conventional MR wrist (superman position). Fat-suppressed (FS) T1 FSE sequences in axial, coronal, and sagittal planes are acquired with 2 mm slice thickness. Additional sequences, T2 fat-saturated coronal, and T1 coronal can be taken.[14]

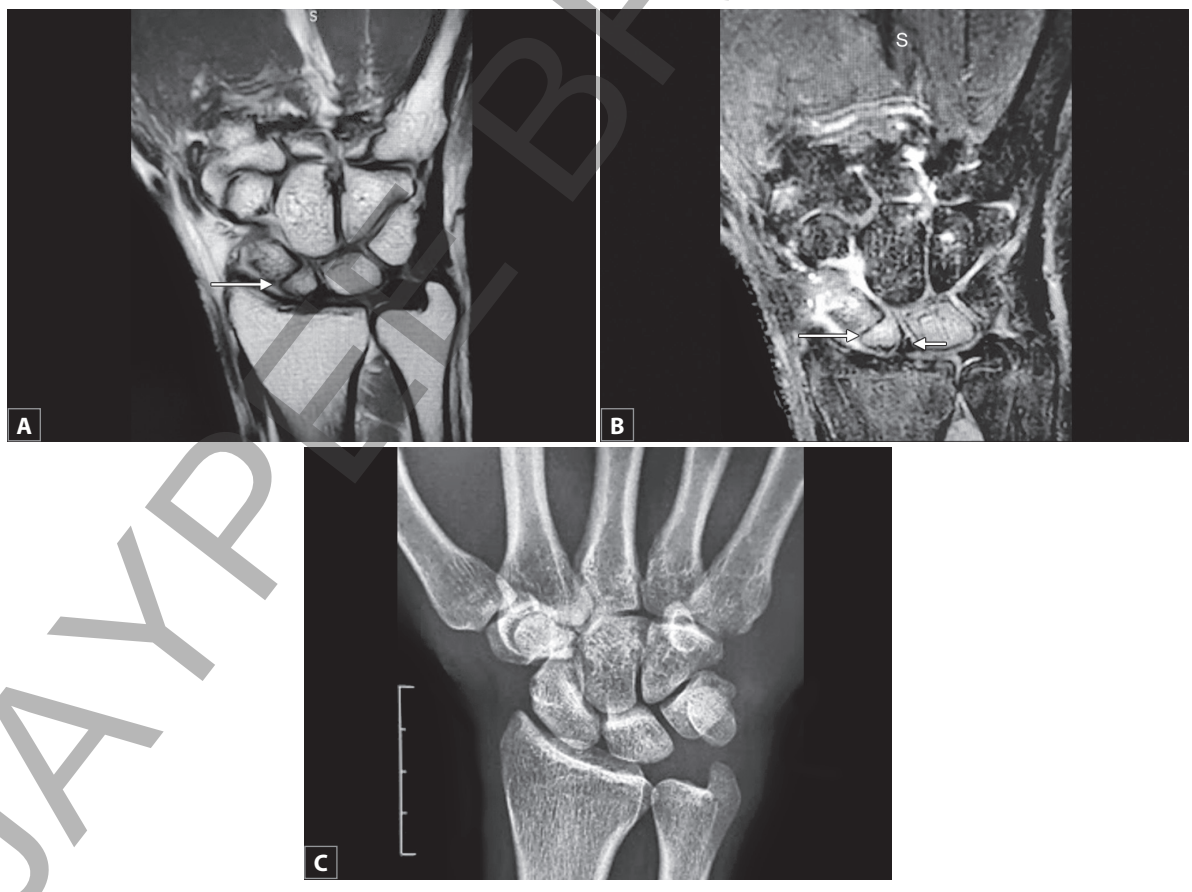
Scaphoid Fracture

Scaphoid is the most common carpal bone to fracture; 70% of the fractures around the carpal bones are scaphoid fractures.

The mechanism of injury is a fall on the outstretched hand with pain in the anatomical snuffbox.

Fractures through the waist of scaphoid are most common.

Fractures through tubercle of scaphoid and incomplete scaphoid waist fractures are stable. Fractures through proximal pole, fracture dislocations, distal pole oblique fractures, and complete fractures through waist are unstable fractures (Herbert classification) **(Figs. 7A to C)**.



FIGS. 7A TO C: Undisplaced proximal pole scaphoid fracture (arrows in A and B) with lunate chondromalacia. The volar scapholunate ligament is intact (small arrow in B). The fracture was not seen on radiographs (C). There is no evidence of avascular necrosis, with normal bone marrow trabecular signal on coronal T1W image (A) and bone marrow edema on T2W coronal fat-saturated image (B).

JAYPEE BROTHERS

The Russe classification divides the fractures according to the orientation of the fracture line—horizontal oblique, vertical oblique, and transverse. The vertical oblique orientation has the most propensity to displace.[15]

However, none of the classifications can predict nonunion.

Clinical symptoms: May be minimal with very little restriction of movement, leading to delay in diagnosis as fractures may be radiologically occult.

Radiographs should be obtained in posterior–anterior and lateral views, hand in 45° ulnar deviation and pronation, and an oblique view in 45–60° pronation.

Radiologically, occult fractures may be evident on computed tomography (CT) or MRI. About 80% of scaphoid is covered by articular cartilage, and the space left for blood supply from the recurrent radial artery branch is minimal. The neglected fractures are at a risk of nonunion due to tenuous blood supply of the scaphoid from the dorsal branch of the radial artery, which enters distal to the waist.[16]

Stable scaphoid fractures are treated conservatively by casts. Delayed union can occur even in stable fractures, which is evident as a persistently visible fracture line 16 weeks after fracture.[17]

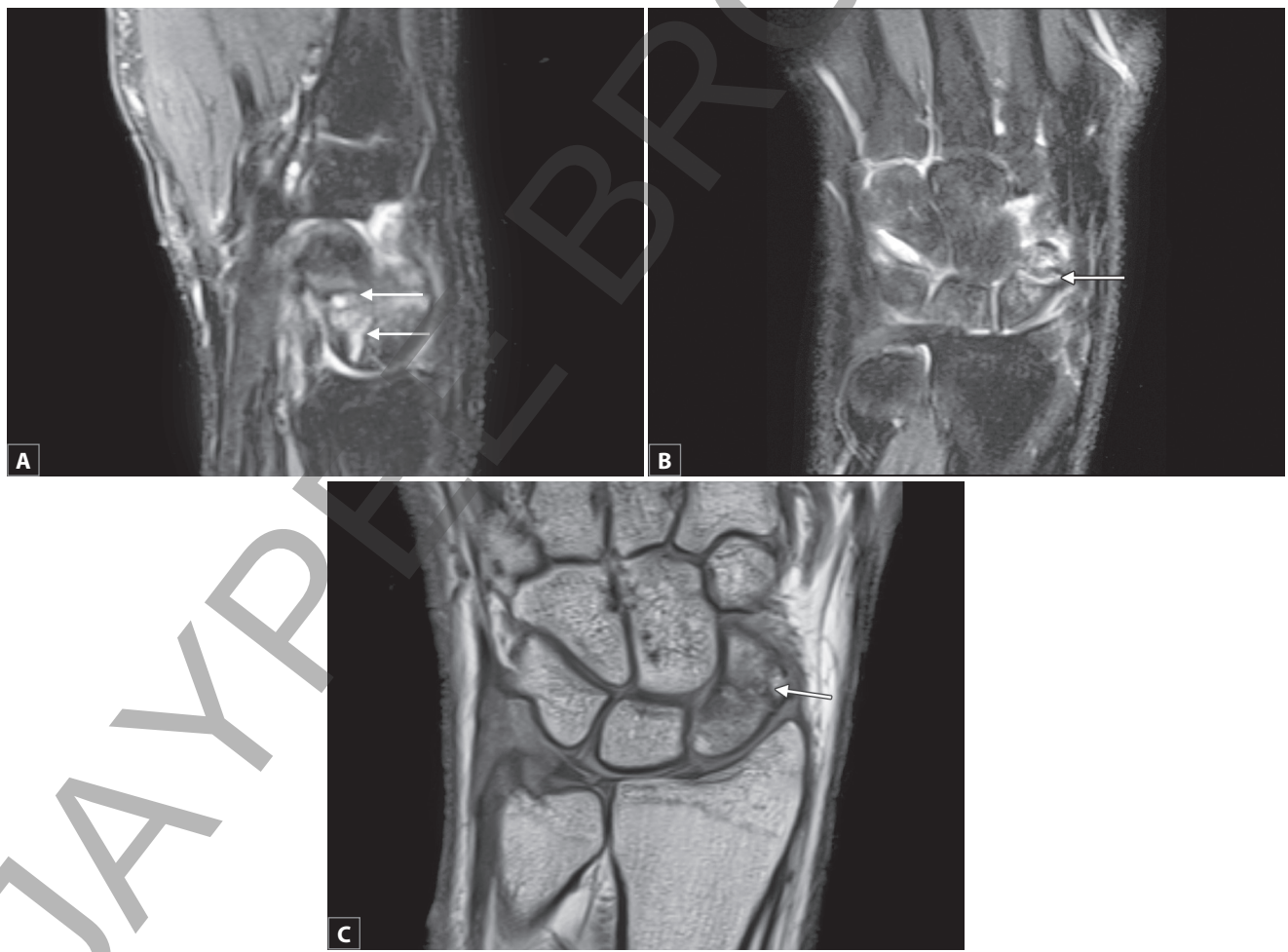
Fractures which do not unite by 6 months are defined as nonunion.[18,19]

Complications of nonunion are avascular necrosis (AVN) of proximal pole of scaphoid, instability, and scaphoid nonunion advanced collapse (SNAC) with progressive osteoarthritis.[18]

Magnetic Resonance Imaging of Scaphoid Injuries

Chronic scaphoid delayed union or nonunion results in sclerosis in radiographs or CT. However, sclerosis does not imply AVN and may be due to neo-osteogenesis.

Presence of sclerosis and fluid in the cleft of the fracture fragment are signs of nonunion on MRI **(Figs. 8A to C)**. MRI is superior to CT or bone scintigraphy in detecting possible AVN due to its superior resolution.



FIGS. 8A TO C: Scaphoid nonunion evident 2 months after trauma. (A) Sagittal and (B) coronal T2W fat-saturated images showing a fluid-filled gap between the fractures through the waist of scaphoid (arrows); (C) A hypointense line is visible on coronal T1W image (arrow).

JAYPEE BROTHERS

The proximal pole is prone to AVN in scaphoid waist fractures due to blood supply from the distal pole traversing through the waist to reach the proximal pole.

Magnetic resonance appearance of hypointensity of >50% of the proximal pole on both T1-weighted (T1W) and T2-weighted (T2W) images suggests AVN.[20]

However, the sensitivity and specificity of noncontrast-enhanced MRI are low in detecting AVN due to a common finding of a heterogeneous signal on T2W images, and hypointensity on both T1W and T2W images is found in ischemic bone **(Figs. 9A to C)**.

Hyperintensity on T2W images may also be present in AVN and hypointensity is seen in only 50% of the cases.[21]

Contrast-enhanced MRI is a useful adjunct to distinguish between ischemic and necrotic bone. Complete lack of enhancement on postcontrast fat-saturated T1W images suggests severe ischemia or AVN.[20,22]

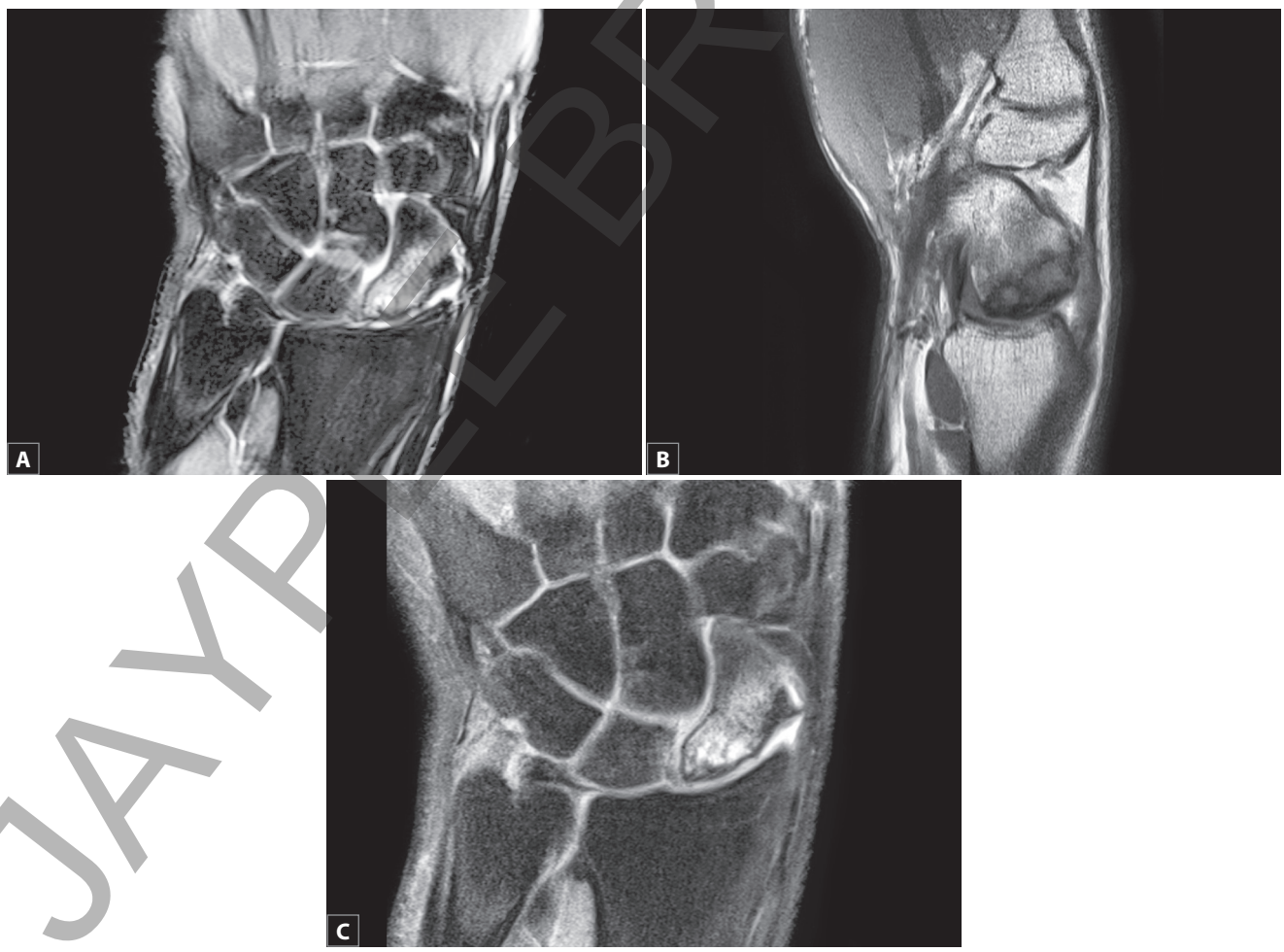
However, some patients with AVN have increased enhancement of the proximal pole on postcontrast images, possibly due to ingrowth of fibrovascular tissue or diffusion of contrast into necrotic bone from the surrounding tissue.[23]

Intraoperative finding of punctate bleeding of a non-necrotic proximal pole is the gold standard to differentiate between AVN and a viable proximal pole.

Diagnostic algorithm: Recent recommendations in imaging of scaphoid fractures suggest that CT be acquired/reformatted in sagittal–oblique and coronal–oblique planes in cases of normal or equivocal radiographs. CT is better in demonstrating a fracture pattern including fracture orientation and dislocation or fragmentation.[24] However, CT is inferior to MRI in detecting microtrabecular fracture and nondisplaced fractures.

Magnetic resonance imaging is useful in detecting all scaphoid fractures, and additional sequences should be acquired in sagittal–oblique and coronal–oblique planes along long axes of scaphoid. However, diagnostic confusion may persist in cases of bone marrow edema (bone contusion) and nondisplaced fracture.[25]

Magnetic resonance imaging is also useful in assessing persistent postoperative nonunion or graft failure. Return of bone marrow signal in the proximal pole is a sign of revascularization.



FIGS. 9A TO C: Scaphoid proximal pole cystic change with bone marrow edema sparing distal pole on proton density (PD)-weighted fat-saturated coronal image (A) with hypointensity of proximal pole on sagittal T1W image (B). However, homogeneous enhancement is seen on postcontrast image (C), suggesting lack of avascular necrosis.

JAYPEE BROTHERS

Fractures of Other Carpal Bones

Fractures of other bones are uncommon. Hook of hamate fractures also occurs due to a fall on the outstretched hand and can occur due to avulsion at the flexor retinaculum attachment site.[16] Hook of hamate fractures can be easily missed on radiographs, where absence of visibility of hook of hamate can be the only sign on routine posteroanterior (PA) views. Ulnar styloid fractures can lead to DRUJ instability, when associated with the base of styloid fractures which disrupt the TFCC. Pisiform is also prone to fractures due to its superficial location and can be detected on routine radiographic views or carpal tunnel view; undiagnosed pisiform fractures lead to pisotriquetral chondromalacia, intra-articular loose bodies, and ulnar nerve impingement.[25]

Kienböck's Disease

Kienböck's disease is referred to AVN of the lunate bone. It was first described by the Austrian radiologist Robert Kienböck in 1910.[26]

The etiology of Kienböck's disease is multifactorial. Predisposing factors include trauma, disruption of venous outflow and local vascular anatomy, ulnar variance, metabolic factors, and repetitive mechanical load. A negative ulnar variance has been found in 78% of cases.[27] Type II lunate with an articulating facet with the hamate also shows a higher risk of Kienböck's disease **(Figs. 10A and B)**.[28]

The terminal arterial branches without sufficient collateral vessels and cases with a single palmar vessel are more prone to Kienböck's disease **(Table 3)**.

The onset of disease is seen between the ages of 20 and 40 years with a 2:1 ratio of men to women. It commonly affects the dominant wrist, but bilateral disease can be seen. The clinical onset can be abrupt or insidious and patients can also remain asymptomatic in the precollapse stage.[29]

Patients present with dorsally located central wrist pain with dorsal tenderness around the lunate, swelling, reduced wrist motion, and grip after acute or repetitive trauma.[30]

Contrast-enhanced MRI helps in differentiation between bone marrow edema and partial or complete necrosis. Enhancement is homogeneous in non-necrotic edematous bone. Partial necrosis shows a heterogeneous enhancement pattern and complete necrosis shows absence of enhancement.[31]

The Lichtman classification may help in treatment decision-making. Options include nonoperative management in early stage disease (stages I to IIIA) to vascularized grafting, proximal row carpectomy, or arthrodesis in late stages (stages IIIB to IV). However, treatment remains controversial and may not alter the natural history of the disease.[32]

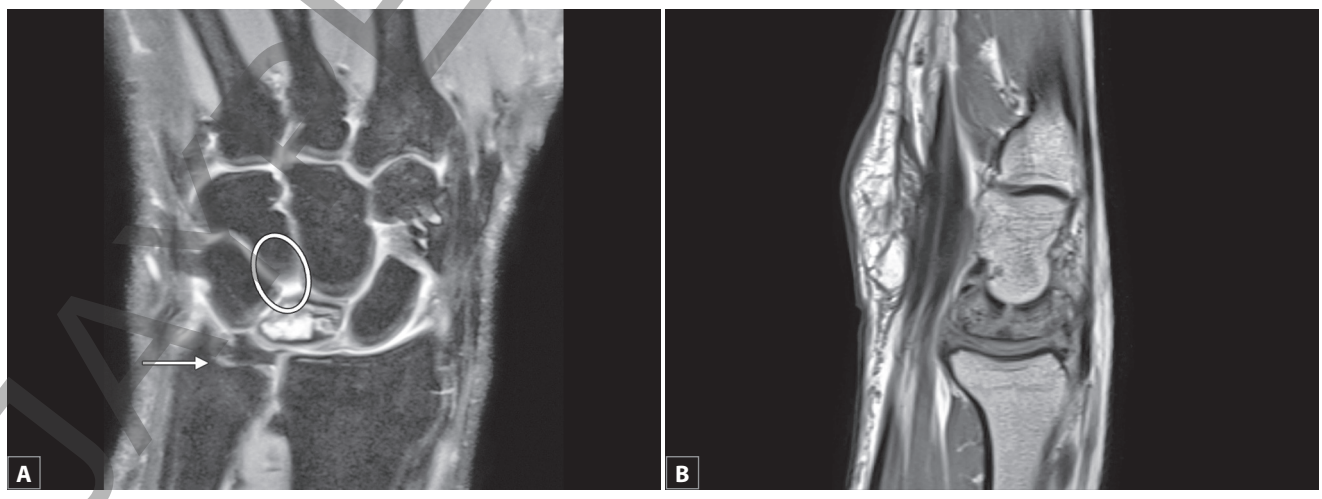
Triangular Fibrocartilage Complex Lesions

Triangular fibrocartilage is a hypointense, biconcave, or bow-tie shaped on coronal sections, discoid or biconcave on sagittal, and triangular on axial sections **(Figs. 11A to C)**.[33] The volar and dorsal radioulnar ligaments of the TFCC have parallel upper and lower margins **(Figs. 12A and B)**.

At the radial attachment, minimal hyperintensity due to hyaline cartilage may be seen and may be mistaken for a tear.[33]

At the ulnar attachment, there are two laminae, one from the styloid process of ulna and one from fovea which are striated but hypointense. Intervening ligamentum subcruentum may appear hyperintense normally.

Triangular fibrocartilage complex lesions can occur due to trauma or repetitive overuse. The Palmer classification



FIGS. 10A AND B: Kienböck's disease with negative ulnar variance with flattened type II lunate. Proton density fat-saturated coronal image (A) showing flattened lunate bone with hyperintensity on fat-saturated images involving the entire lunate (A) and hypointensity of the lunate on the T1W image (B). The lunate has a facet for articulation with hamate (oval in A). The articular surface of distal ulna is proximal to that of the radius (negative ulnar variance) (arrow in A), another predisposing factor for Kienböck's disease.

JAYPEE BROTHERS

TABLE 3: Lichtman staging of Kienböck's disease.[31]		
Stages	***Radiographic and CT findings***	***MRI findings***
I	Normal morphologic findings	• Morphologic preservation • Edema pattern in bone marrow
II	• Normal morphologic findings • Sclerosis in bone marrow	• Morphologic preservation • Signal intensity low on T1W images, variable on T2W images
IIIA	• Collapse of lunate bone • Radioscaphoid angle <60°	• Morphologic collapse of lunate bone • Signal intensity low on T1W images, variable on T2W images
IIIB	• Collapse of lunate bone • Radioscaphoid angle >60°	• Morphologic collapse of lunate bone • Signal intensity low on T1W images, variable on T2W images
IIIC	• Collapse of lunate bone • Coronal lunate fracture (chronic)	• Morphologic collapse of lunate bone • Signal intensity low on T1W images, variable on T2W images Coronal lunate fracture (chronic)
IV	Radiocarpal or midcarpal degenerative arthritis	• Radiocarpal or midcarpal degenerative arthritis • Signal intensity low on T1W images, variable on T2W images

TABLE 4: Classification of triangular fibrocartilage complex (TFCC) tears.	
Class I tears (traumatic)	
IA	Central perforations
IB	Ulnar avulsion with or without distal ulnar fracture
IC	Distal avulsion at carpal attachment
ID	Radial avulsion with or without sigmoid notch fracture
Class II tears (degenerative)	
IIA	TFCC wear
IIB	TFCC wear with lunate and/or ulnar chondromalacia
IIC	TFCC perforation with lunate and/or ulnar chondromalacia
IID	C and lunotriquetral ligament perforation
IIE	D and ulnocarpal arthritis

divides TFCC injuries into two classes: Traumatic (Class I) and degenerative (Class II) **(Table 4)**.[25]

However, the Palmer classification does not classify tears of volar or dorsal radioulnar ligaments or subclassify type IB ulnar avulsions further into distal (styloid) avulsions or proximal (foveal) avulsions, which have prognostic and therapeutic significance, since the foveal attachment damage is more disabling and styloid avulsion fractures associated with distal lamina tears can cause instability. Combinations of different tears and partial tears are also common and have not been classified.[34]

Type IA tears are central perforations of the TFC, often found in asymptomatic individuals and do not result in any dysfunction of the DRUJ. Central perforations are seen as fluid-signal intensity or contour irregularity within the central or paracentral portion of the triangular fibrocartilage proper and may be partial-thickness tear of either the proximal or the distal (less common) articular surface. Type IA tears are in the avascular zone and cannot be surgically repaired **(Figs. 13A and B)**.

Type IB tears near the ulnar attachment are difficult to diagnose on MRI; features of ulnar-sided synovitis and focal fluid on the ulnar side are clues to diagnosis. Ulnar-sided tears and type IC tears are vascular and respond well to interventions.[34] MR arthrography with DRUJ injections have better sensitivity in detecting type IA and IB lesions **(Figs. 14A and B)**.

Type IC tears appear as thickening with edema within the ligament on long TE sequences.[34] Type ID tears near the radial attachment can be associated with radial avulsion fractures of sigmoid notch.

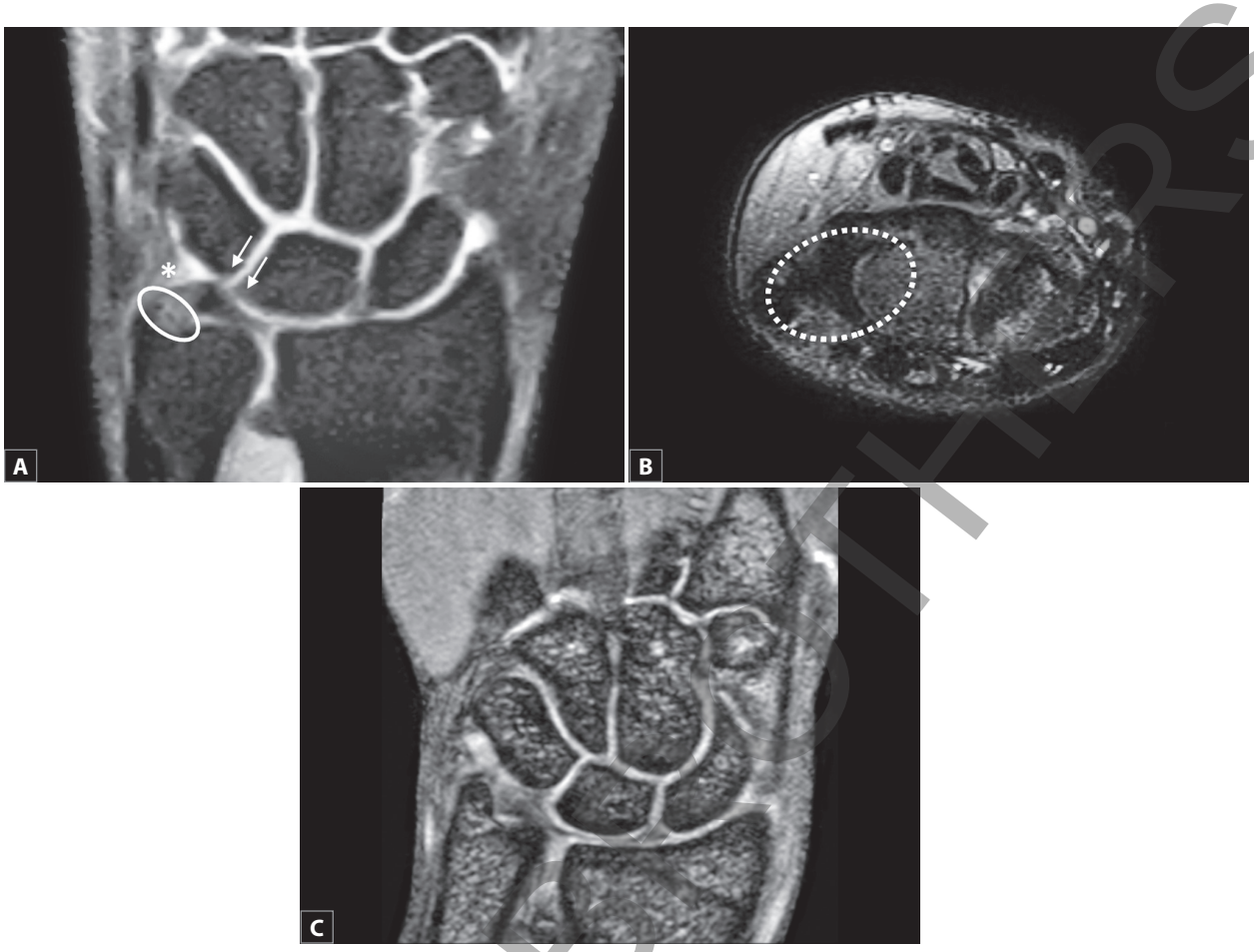
Degenerative Tears

Triangular fibrocartilage complex degeneration manifests as intrasubstance hyperintensity not communicating with the articular surface. The disc may appear diffusely thinned in degenerative tears. Degenerative tears are common with aging and rarely seen before 30 years and are associated with positive ulnar variance and ulnar impaction with chondromalacia of lunate or degenerative subchondral cysts.[34]

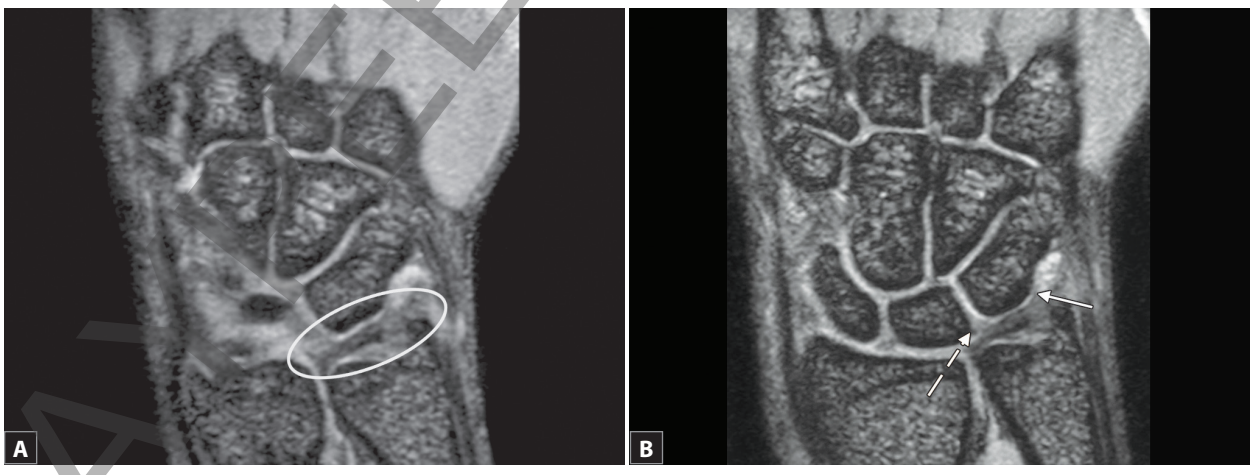
Three-Dimensional Imaging

Three-dimensional isotropic imaging is specifically useful for evaluating the TFCC since in the imaging position, the TFCC is not orthogonal to the coronal plane but oblique to it, resulting in false-positive diagnosis of tears as the entire ligament may not be visualized in one section due to its obliquity. 3D sequences with a section thickness of 1 mm or less with no interslice gap can be reconstructed with multiplanar reconstructions for better evaluation of the TFCC. Punctate hypointensity on 3D gradient echo sequences is an early sign of degeneration.[35]

JAYPEE BROTHERS



FIGS. 11A TO C: Normal triangular fibrocartilage complex (TFCC): Hyperintensity on coronal T2W fat-saturated image (A) at radial and ulnar (oval) attachment sites. Central disc is biconcave and hypointense on coronal sections and seen as triangular in axial sections (dashed oval in B). Meniscal homologue (asterisk), ulnolunate, and ulnotriquetral ligaments (arrows in A) are seen. Appearance of the TFCC on coronal gradient echo sequence (C).



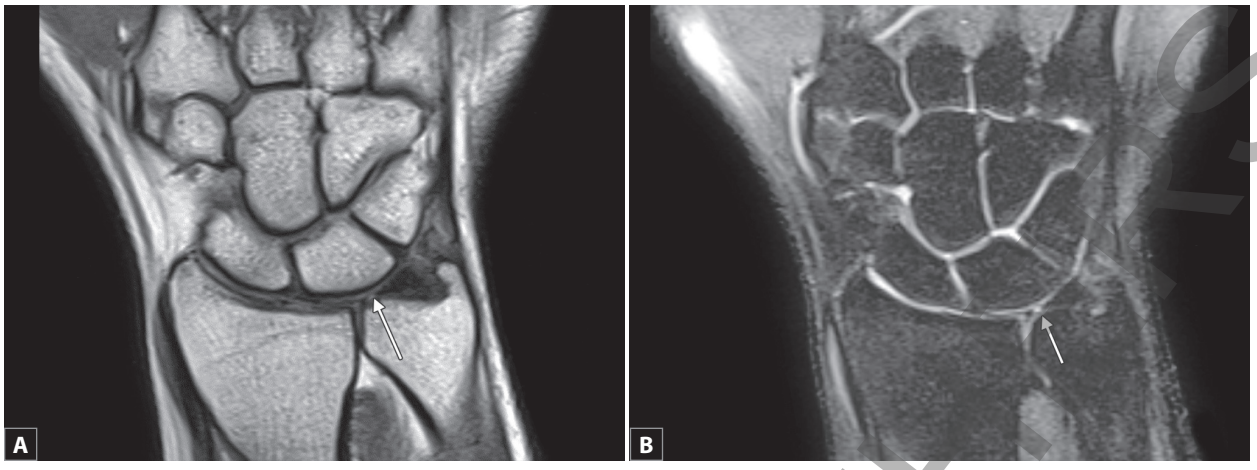
FIGS. 12A AND B: (A) Dorsal radioulnar ligament (oval) which has horizontal superior and inferior margins unlike the biconcave triangular fibrocartilage articular disc proper; (B) Ulnolunate (dashed arrow) and ulnotriquetral ligaments (arrow).

Radioulnar Ligament Lesions

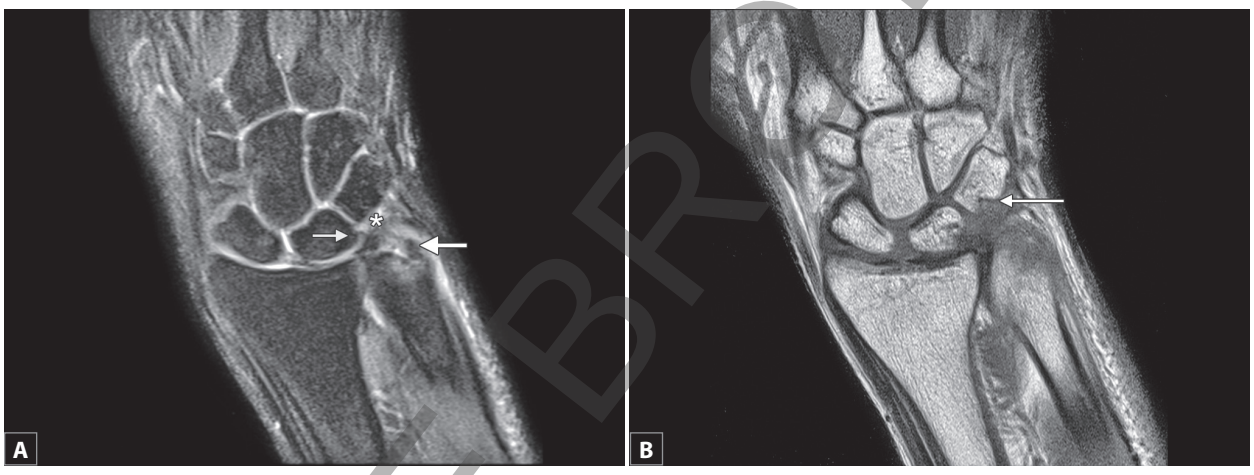
Injuries of dorsal and volar radioulnar ligaments result in DRUJ dysfunction with ulnar-sided wrist pain.

The dorsal and volar radioulnar ligaments have flat superior and inferior margins unlike the biconcave margins of the TFC and are hypointense on all pulse

JAYPEE BROTHERS



FIGS. 13A AND B: Central triangular fibrocartilage complex (TFCC) tear. Coronal proton density-weighted (A) and T2W fat-saturated (B) images showing a central perforation of the TFCC (arrow), with fluid signal within the central portion of the disc. These tears are often asymptomatic.



FIGS. 14A AND B: (A) Proton density-weighted fat-saturated coronal MRI revealing fracture of base of ulnar styloid (thick arrow) with thickened and hyperintense proximal and distal lamina of triangular fibrocartilage (TFC) (thick arrow). The ulnolunate ligament is hypointense (thin arrow). Hyperintensity and thickening of ulnotriquetral ligament are seen (asterisk). (B) Coronal T1W image showing osteochondral impaction injury at the proximal radial side of triquetrum (arrow) at the ulnolunate ligament attachment site.

sequences, but mildly more hyperintense than the triangular fibrocartilage (TFC) proper.

Disruptions of the radioulnar ligaments should be carefully evaluated on the peripheral MRI sections. The ulna commonly subluxates dorsally relative to the sigmoid notch due to tear of the dorsal radioulnar ligament with loss of concentric relation between sigmoid notch of radius and ulnar head **(Figs. 15A to C)**.[33]

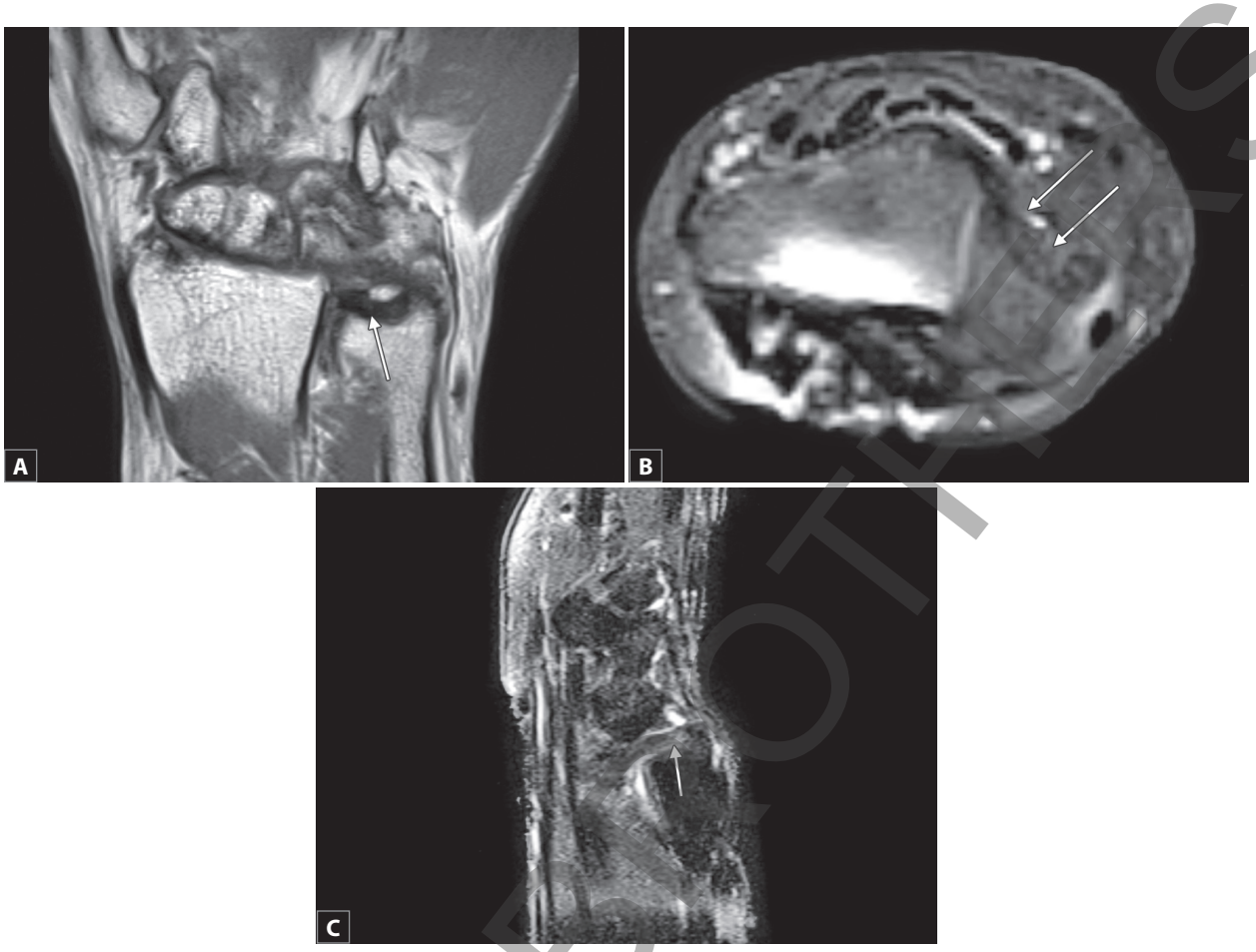
Ulnar Impaction Syndrome (Ulnocarpal Abutment)

Ulnar impaction syndrome is a common cause of ulnar-sided wrist pain and is occasionally associated with positive ulnar variance causing excessive load on the ulnar side of the wrist with ulnar impaction on the TFCC and ulnar-sided carpal bones. The condition can also be seen in neutral or negative ulnar variance.[25]

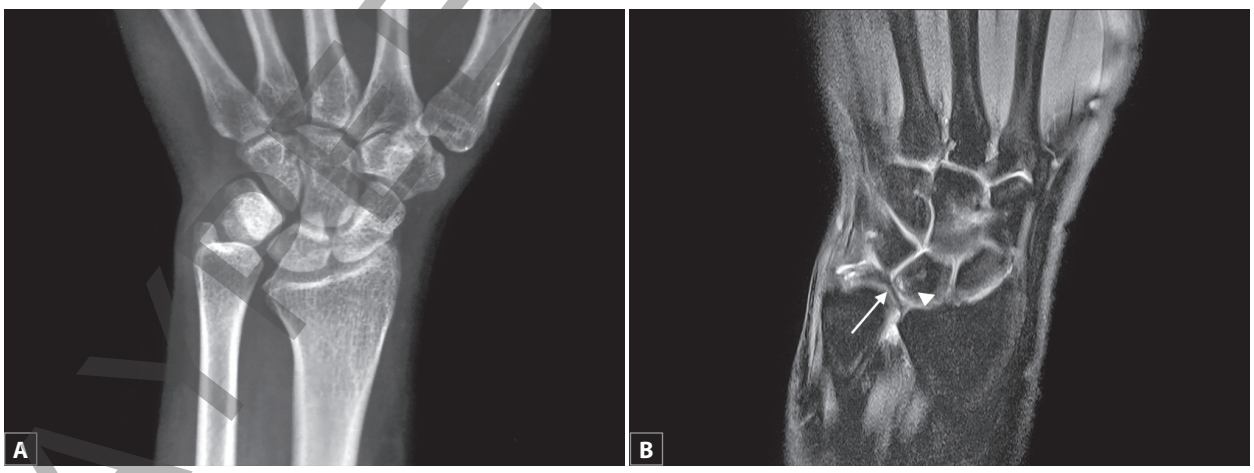
Radiography with forearm in pronation with hand gripped may show the actual increase in positive ulnar variance and impaction. Foreshortened radius may also be found postsurgically, post-traumatically in malunited foreshortened radius, due to premature physeal fusion of the distal radius (congenitally or in post-traumatic cases in skeletally immature patients).[2,25]

Magnetic resonance imaging is useful in detecting early changes since radiographic findings may be subtle or normal even in advanced disease. MRI shows the ulnar-sided degenerative changes involving ulnar-sided carpal bones (ulnar side of lunate, triquetrum) and ulnar head. Cartilage thinning, subchondral cysts, marrow edema, and sclerosis along the ulnar aspect of the lunate and/or triquetrum may be seen **(Figs. 16A and B)**.[25] Degenerative changes in the thinned-out TFCC are also seen. Advanced cases lead to ulnocarpal joint arthritis.

JAYPEE BROTHERS



FIGS. 15A TO C: Radial-sided triangular fibrocartilage complex tear. On the (A) coronal T1W, (B) axial T2W fat-saturated, and (C) sagittal T2W fat-saturated images, the volar radioulnar ligament is thickened (arrows), with negative ulnar variance. (B) The dorsal radioulnar ligament is torn. (C) Dorsal ulnar subluxation is present.



FIGS. 16A AND B: Ulnocarpal abutment. (A) Radiograph and (B) Coronal T2W fat-saturated image. Positive ulnar variance with thinned-out triangular fibrocartilage (TFC) and chondromalacia along the ulnar aspect of the lunate (arrowhead).

Ulnar Styloid Impaction Syndrome

Ulnar styloid impaction syndrome causes ulnar-sided wrist pain due to impaction between a long styloid process of ulna (>6 mm) and a nonunited styloid process fracture fragment and the triquetral bone.

Magnetic resonance imaging findings: Degenerative changes are noted in a long or curved ulnar styloid process and in triquetrum with bone marrow edema, cartilage changes, subchondral cysts, and sclerosis along the styloid process and triquetrum **(Fig. 17)**.[25]

JAYPEE BROTHERS

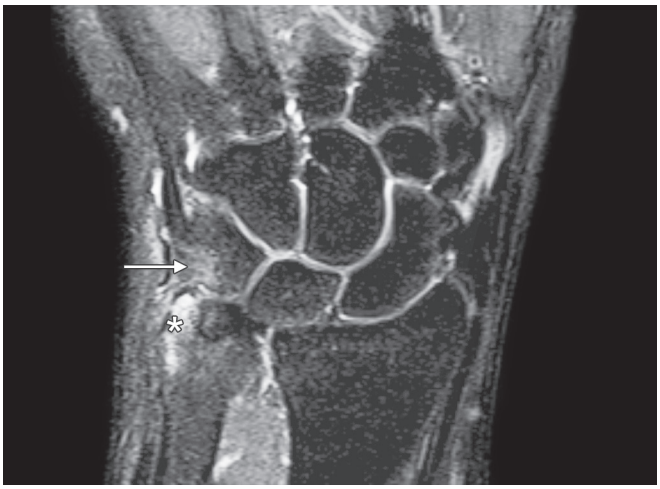


FIG. 17: Coronal T2W fat-saturated image showing ulnar styloid impaction with edema of the ulnar styloid process (asterisk) and ulnar aspect of triquetrum (arrow).

Ulnar Impingement Syndrome

In this condition, a shortened ulna, which lies proximal to the sigmoid notch, impinges against the radius. MRI shows a foreshortened ulna with bone marrow edema at the level of impingement on the radius proximal to sigmoid notch. Later stages show sclerosis, scalloping along the ulnar margin of distal radius, and degenerative changes with osteophytes.[25]

Hamatolunate Impingement

Hamatolunate impingement occurs due to a type II lunate where there is an additional facet on the distal articular surface of the lunate where the hamate and lunate articulate. Impingement at this articulation can cause chondromalacia and pain.[36]

Carpal Instability

Carpal instability is defined as the inability to bear physiological load.

Carpal instabilities are most commonly caused by injuries to the intrinsic ligaments of the wrist, though inflammatory and congenital conditions can also lead to instability. Based on the type of injury, carpal instability is classified into four types according to the Mayo classification **(Table 5)**.

Carpal Instability Dissociative

Scapholunate instabilities are the most common carpal instabilities, and the scapholunate and lunotriquetral ligament injuries are the most common causes of dissociative carpal instability. Scaphoid fractures, Kienböck's disease, and rheumatoid arthritis (RA) also cause scapholunate instability.[37]

TABLE 5: Classification of carpal instability.

Nomenclature	*Area of abnormality*
Carpal instability dissociative (CID)	Between the proximal row (most common) and distal row of carpal bones in the same row
Carpal instability nondissociative (CIND)	Between radiocarpal and midcarpal rows
Carpal instability complex	Combination of the above two
Adaptive carpus	Due to abnormality proximal or distal to carpal rows

Scapholunate ligament injury: Scapholunate ligament injuries are associated with radial-sided wrist pain and popping or clicking on physiological loading of the wrist joint. Scapholunate ligament injury can result in scapholunate dissociation, scapholunate advanced collapse (SLAC), and SNAC.[38]

The scapholunate ligament has three components: Dorsal, interosseous, and volar. The dorsal component is most important for maintaining stability. The dorsal intercarpal ligaments also act as secondary stabilizers.[39]

Scapholunate dissociation causes widening of the scapholunate interval to >3 mm on radiographs. This is known as Terry Thomas sign. However, routine radiographs may be normal even in complete scapholunate ligament tears and stress radiographs may be required with clenched fist views or wrist in ulnar and radial deviation. MRI or MR arthrography can demonstrate the ligament tear.

Scapholunate ligament injuries cause a pattern of injury known as dorsal intercalated segment instability (DISI) with a dorsal tilt of the concave distal articular surface of the lunate and volar tilt of the scaphoid with an increase in the scapholunate angle (>60°). These injuries occur due to damage to scapholunate ligament along with secondary stabilizers such as radioscaphocapitate and scaphocapitate ligaments.[37,38]

Further progression leads to degenerative changes in the radioscaphoid articulation and ultimately carpal collapse **(Figs. 18A to C)**. Nontraumatic scapholunate dissociation and SLAC are seen in patients with calcium pyrophosphate deposition disease.

On MRI, partial tears may appear as an elongated or a focally thin ligament or a focal area of high-signal intensity. Complete tears appear as a complete discontinuity.[13] Double-compartment MR arthrography can demonstrate tears with greater sensitivity and specificity.[13,40]

Lunotriquetral ligament injury: The lunotriquetral ligament, like the scapholunate ligament, has three components (dorsal, interosseous, and volar) and plays an important role in maintaining stability of the proximal carpal row. The volar component of the lunotriquetral ligament is the strongest. Lunotriquetral ligament injuries present with ulnar-sided wrist pain.

JAYPEE BROTHERS



FIGS. 18A TO C: Tear of the volar scapholunate (Sc) ligament with fluid signal cleft at lunate (Lu) attachment (arrow in A and B). The ligament is hyperintense and thickened (A). The interosseous and dorsal scapholunate ligaments are normal (oval in B). Radioscaphoid joint arthritis with spur projecting from the radial styloid process seen abutting the scaphoid (oval in C).

JAYPEE BROTHERS

Lunotriquetral ligament injury along with injury of the secondary stabilizers (dorsal radiotriquetral and dorsal scaphotriquetral ligaments) leads to volar intercalated segment instability (VISI). The lunate rotates in a volar direction.[41]

The lunotriquetral ligament is triangular or linear. The tears of this ligament are not easily detected on MRI, and MR arthrography has greater sensitivity in detecting tears. Widening of the lunotriquetral interval is rarely seen, unlike scapholunate ligament tears.[13]

Distal Radioulnar Joint

The distal radius, ulna, TFCC, and joint capsule form the DRUJ. The head of ulna forms a pivot joint after it articulates with the sigmoid notch on the ulnar aspect of the distal radius. Forearm movement of pronation and supination occur at the DRUJ, which also plays an important role in stabilization of the forearm. The foveal attachment of the radioulnar ligaments of the TFCC and the ulnotriquetral ligament also have a role in maintaining stability. Distal radial fractures are also associated with DRUJ injuries, which often go unrecognized.[42]

The clinical features of DRUJ instability include pain or audible clicking on pronation/supination or restricted movement. The empty groove of ECU can be palpated. The ulna which subluxates dorsally can also be palpated.[42]

Associated osseous injuries—Colles', Smith's (reverse Colles, fracture), Essex-Lopresti, Galeazzi, Chauffeur's, and Barton's fractures—can be associated with DRUJ instability. DRUJ instability causes ulnar-sided pain and early onset of degenerative arthritis in patients with distal radial fractures.[14,42]

Radiography is the primary investigation of choice and in a well-positioned lateral radiograph, the ulnar anterior and posterior margins overlap with the radius. However, positioning may be difficult and subtle subluxations may be missed.

The CT and MRI are useful for detecting the congruence of the DRUJ on axial images. In addition to ligamentous and osseous injuries, entrapment of ECU may also be

detected, which may result in failure of closed reduction in certain osseous injuries such as Barton's fracture.[43]

Post-traumatic fractures of ulnar styloid, especially base of ulnar styloid, are also associated with DRUJ instability due to concomitant injury to foveal attachment of TFCC. Chronic unstable styloid fractures or malunited ulnar styloid fractures also result in repetitive trauma and dislocation or tears of ECU. Post-traumatic distal radial fractures and physeal fusion can lead to positive ulnar variance and DRUJ instability due to TFCC tears.[42]

Tendon Disorders

Tendons have low-signal intensity on all pulse sequences due to a parallel arrangement of fibers with low water content. APL can have a normally striated appearance due to multiple tendon slips with interspersed fat. Magic angle artifact can cause artifactual intermediate-signal intensity, especially in the FPL and ECU.[44]

De Quervain's Tenosynovitis

De Quervain's tenosynovitis affects the first extensor compartment containing the APL and EPB. This is commonly seen in middle-aged females and can be bilateral in 30%.[44] It is also common in the peripartum period.[33] Positive Finkelstein's test with pain on ulnar deviation of the thumb is diagnostic.

The MRI findings include tendon thickening, fluid around the tendon sheath, and surrounding edema. A septum may be found between the tendon sheaths **(Figs. 19A and B)**. Ultrasound is an alternative tool to MRI to look for septum between the two tendons.

Intersection Syndrome

The first compartment tendons of APL and EPB cross from ulnar to radial side over the second compartment extensor tendons of extensor carpi radialis longus and brevis. Overuse or repeated friction at this intersection 3–4 cm proximal to Lister's tubercle of the radius causes tenosynovitis of the second compartment with pain in the distal forearm. The site of pain is proximal to the site of pain in de Quervain's tenosynovitis, at the site of intersection. Overhead racket players and weightlifters are prone to this overuse injury.

Distal Intersection Syndrome

Distal intersection syndrome is a rare cause of pain on the dorsal side of the wrist over Lister's tubercle at the point of crossing of the third compartment tendon of EPL over the second compartment tendons of extensor carpi radialis brevis and longus.

Extensor Carpi Ulnaris Tenosynovitis

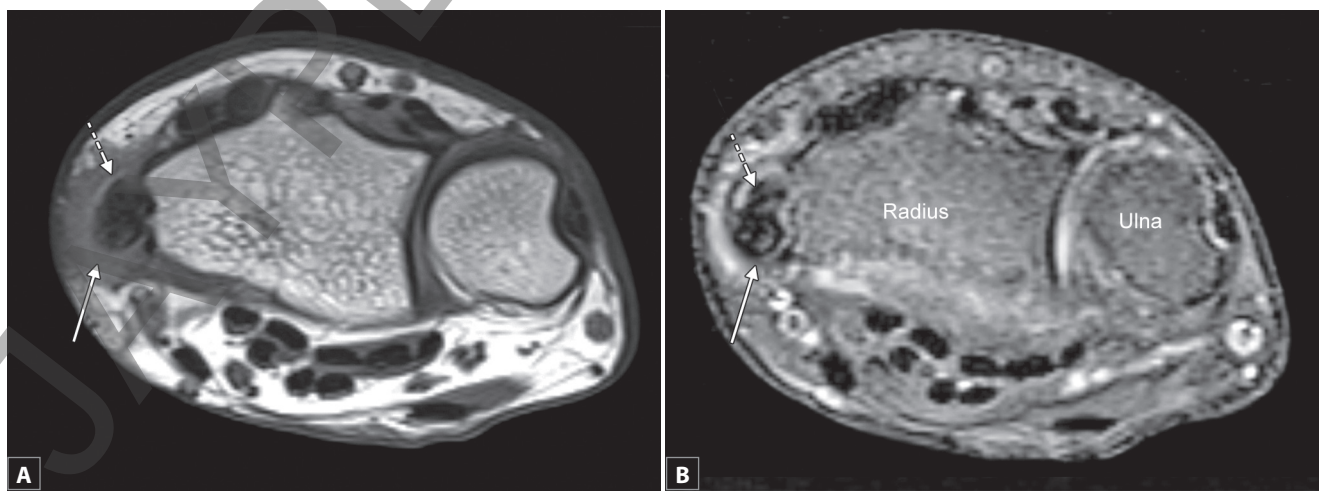
Extensor carpi ulnaris tenosynovitis is common and seen most commonly in patients with RA and in patients with subluxation of the ECU due to DRUJ instability, which may be postinflammatory or post-traumatic **(Figs. 20A and B)**.

Flexor Tenosynovitis

Flexor tenosynovitis occurs commonly in patients with RA or tubercular arthritis, both of which can lead to synovial thickening and intrasynovial rice bodies. Distension of the common flexor tendon sheath can present as carpal tunnel syndrome (CTS) **(Figs. 21A and B)**.

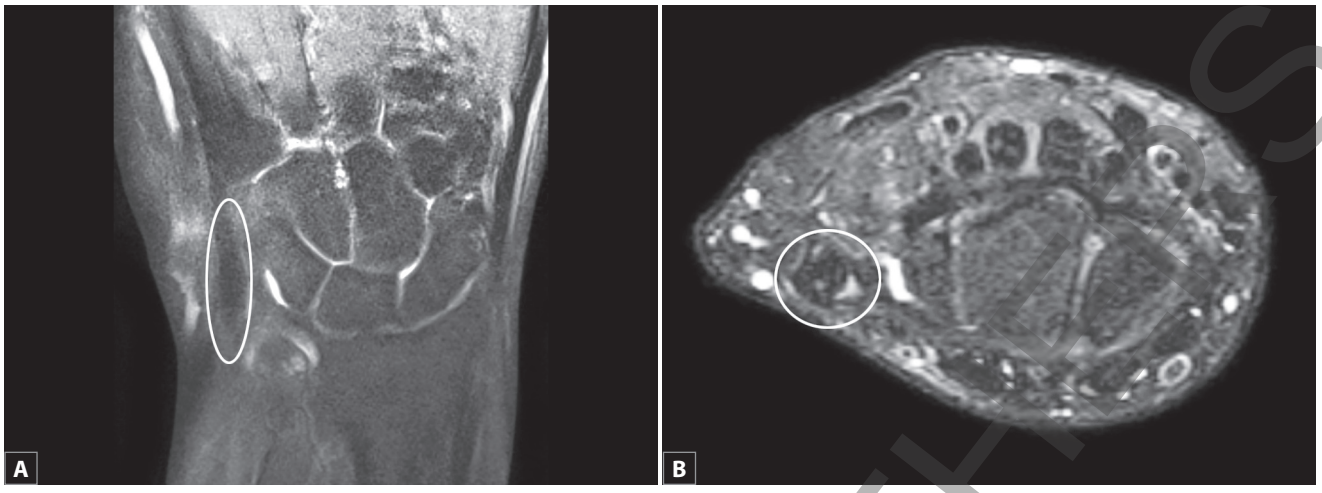
Carpal Tunnel Syndrome

Carpal tunnel syndrome accounts for approximately 90% of all entrapment neuropathies and is caused by compression of the median nerve at the carpal tunnel

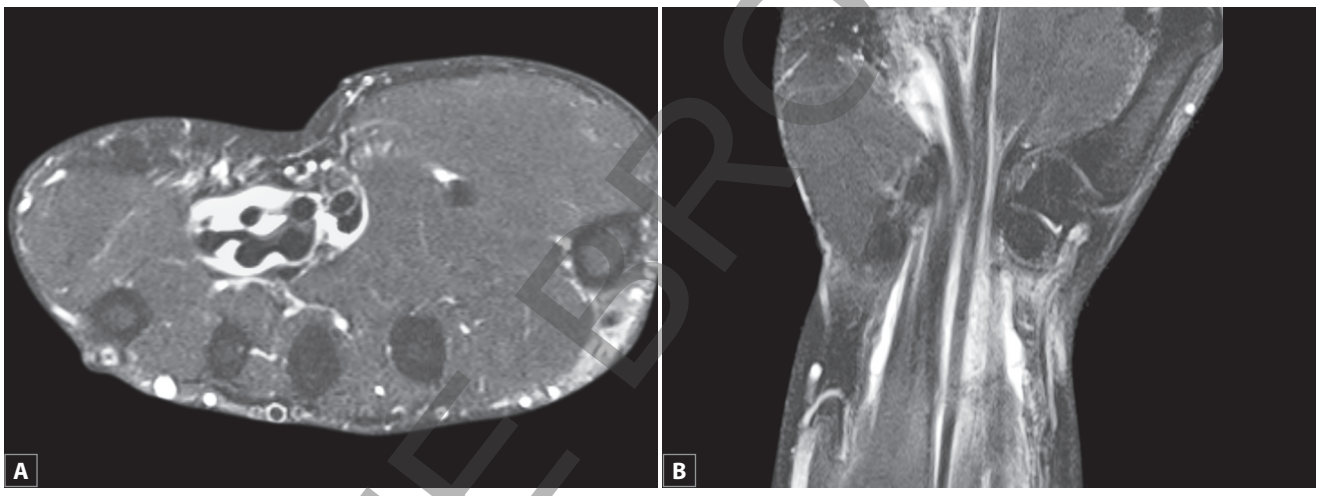


FIGS. 19A AND B: De Quervain's tenosynovitis. (A) Axial T1W and (B) T2W fat-saturated images show thickening and intratendinous intermediate signal of abductor pollicis longus (arrow) and extensor pollicis brevis (dashed arrow). Fluid seen surrounding the tendons and mild surrounding soft-tissue edema are also present.

JAYPEE BROTHERS



FIGS. 20A AND B: Flexor carpi ulnaris tendinopathy in a patient with ulnar wrist pain. Coronal proton density-weighted fat-saturated images show a focal thickening of flexor carpi ulnaris with mild fluid (ovals in A and B). Fluid is also seen in the adjacent distal radioulnar joint.



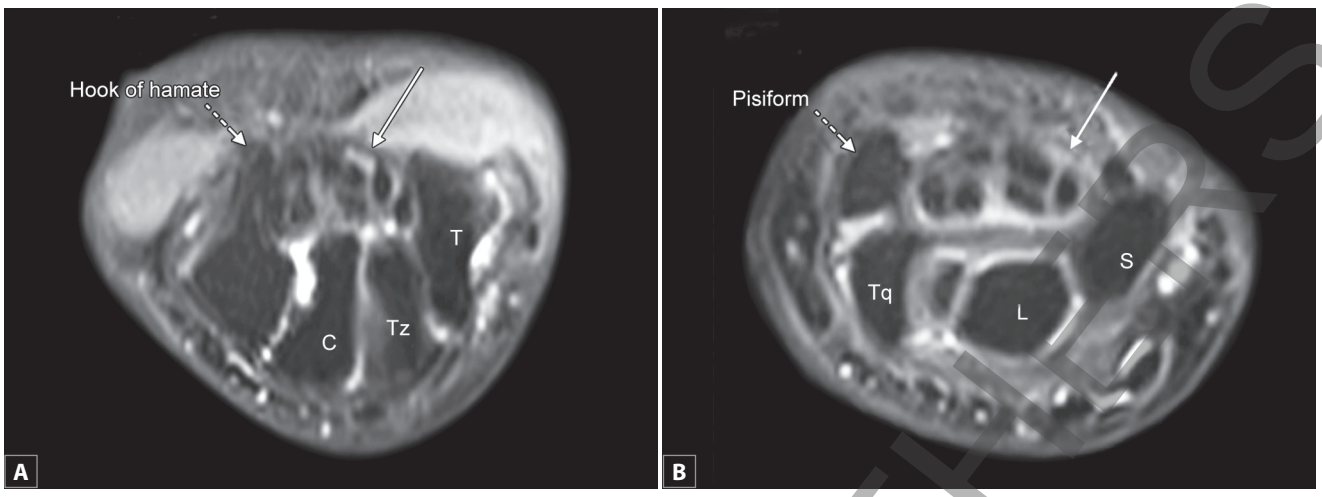
FIGS. 21A AND B: Flexor tenosynovitis. Fluid is seen around the flexor tendons in the (A) axial and (B) coronal T2W fat-saturated sequences.

in the volar aspect of the wrist. Patients present with complaints of pain, numbness, or tingling feeling in the hands in the median nerve distribution.[45] Nerve conduction studies remain the gold standard for diagnosing and grading CTS, but provide limited information about the exact location, extent, and possible cause of nerve entrapment and is also uncomfortable for the patient.[46] Magnetic resonance neurography (MRN) is a specific MR technique to enhance the peripheral nerve visualization with the help of high-resolution and high-contrast pulse sequences. MRI has the advantages of excellent soft-tissue resolution and the capacity to delineate the site of nerve injury and demonstrate the secondary causes of CTS.[47]

Magnetic resonance neurography sequences that were recommended include axial T1W pulse sequence, axial FS pulse sequence, preferably T2-spectral adiabatic inversion recovery (SPAIR) sequence, coronal proton density sequence, and 3D nerve imaging.[48] The advantage of the 3D isotropic technique lies in the ability to allow thinner slices and multiplanar reconstructions derived from isotropic voxels for clear display of nerves along the long axis. A diffusion-based 3D reversed fast imaging with steady-state free precession (3D PSIF) is another sequence which can be used to cause vascular signal suppression in peripheral nerves creating nerve-specific images.[44,45] Diffusion tensor imaging can also be performed for quantification of the fractional anisotropy (FA). Axial T2 SPAIR sequence is adequate for assessing the median nerve; T2 fat-suppressed 3D PSIF sequence is useful to delineate the margins and course of the median nerve.[49]

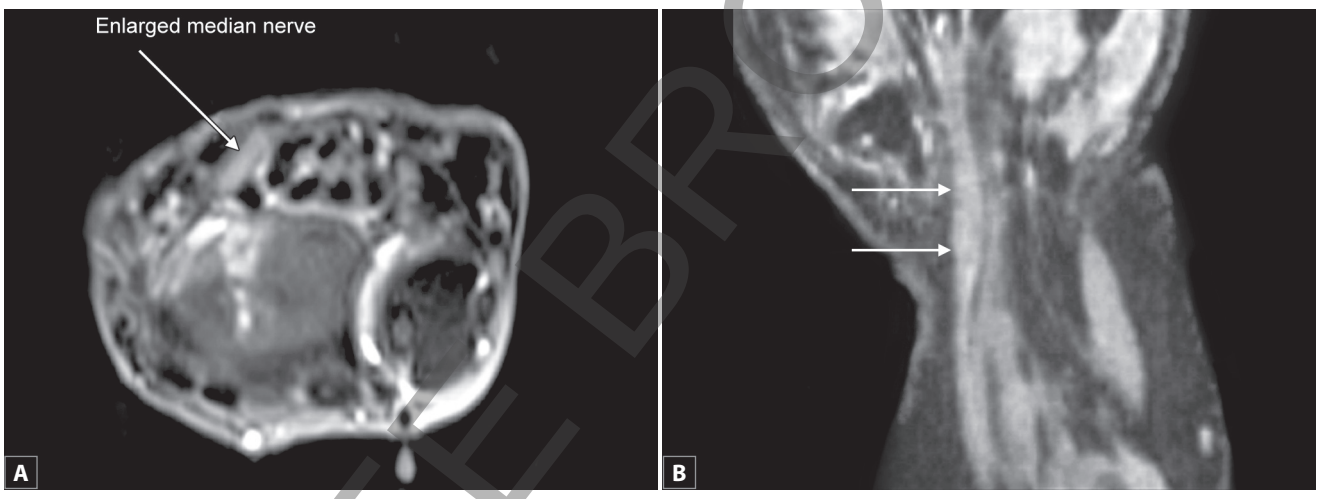
Cross-sectional area (CA) of the median nerve is the most well-studied parameter, with measurement just proximal to the tunnel or at the site of the most marked swelling of the nerve being the most useful.[50-53] A cutoff

JAYPEE BROTHERS



FIGS. 22A AND B: Normal median nerve on MRI. Axial T2 SPAIR images at the (A) hamate hook level (dashed arrow in A), (B) level of pisiform bone (dashed arrow in B) depicting normal size and signal intensity of the median nerve (arrow) at the CT in the right wrist of a patient in the control group.

(C: capitate, L: lunate; R: radius; S: scaphoid; SPAIR: spectral adiabatic inversion recovery; T: trapezium; Tq: triquetrum; Tz: trapezoid; U: ulna)



FIGS. 23A AND B: (A) T2 SPAIR axial image showing enlarged median nerve; (B) 3D PSIF curved reformatted image showing focal thickening of the median nerve just proximal and at the carpal tunnel in a patient with severe CTS on nerve conduction studies.

(CTS: carpal tunnel syndrome; PSIF: reversed fast imaging with steady-state free precession; SPAIR: spectral adiabatic inversion recovery)

value of CA of >0.165 cm^2, 1 cm proximal to the pisiform, had the highest sensitivity of 91.1% and specificity of 87.5% **(Figs. 22A and B)**.[49] Koh et al. found a value of 0.143 cm^2 at the same level to give a sensitivity of 76.2% and specificity of 73.8%.[50] Klauser et al. found a cutoff value of 0.575 for FA to have sensitivity and specificity of 73.9 and 80%, respectively, and a maximum CA value of 0.17 cm^2 to have a sensitivity of 93.3% and specificity of 93.3%.[54]

Median nerve signal intensity on MRI relative to the hypothenar muscle is significantly different between patient and control group **(Figs. 23A and B)**.[50,55] Retinacular bowing of >0.122 cm has a sensitivity and specificity of 60.0 and 65.6%, respectively.[49] Associated findings of extraosseous ganglion cysts and flexor tenosynovitis may be found.

Guyon's Canal Syndrome

Guyon's canal syndrome is a rare ulnar neuropathy. The ulnar nerve while traversing through the narrow Guyon's canal in the wrist can be compressed by ganglion cysts. Repetitive trauma can cause ulnar artery thrombosis or aneurysm, a condition known as hypothenar hammer syndrome.[56]

Wartenberg's Syndrome

Wartenberg's syndrome is pain or paresthesia along the radial aspect of dorsal forearm and over dorsal thumb and index finger due to injury or compression of the superficial radial nerve, which emerges and courses between the brachioradialis and extensor carpi radialis longus tendon.

JAYPEE BROTHERS

Inflammatory Arthritis

Rheumatoid Arthritis

Changes of RA can be detected early before radiographic evidence of the disease by both ultrasound and MRI, as early as 4 months from clinical onset. Synovitis, erosions, and tenosynovitis can be detected by both modalities. However, MRI can also reveal bone marrow edema, which is a precursor of erosions **(Figs. 24A to C)**.[57]

Contrast-enhanced MRI can differentiate between synovitis, which enhances, and effusion, which is nonenhancing. However, in late acquisitions, gadolinium can diffuse into the synovial fluid and this occurs more rapidly in small joint.[58] Dynamic gadolinium-enhanced MRI can quantify the degree of synovial enhancement. The extent of erosions and bone marrow edema on MRI can also be used for longitudinal follow-up and assessment of response.

Synovitis, erosions, and bone marrow edema can be graded with scores of 0–3 according to the Outcome Measures in Rheumatology Clinical Trials (OMERACT) and European League Against Rheumatism (EULAR) Rheumatoid Arthritis Magnetic Resonance Imaging Score (RAMRIS) system.[59]

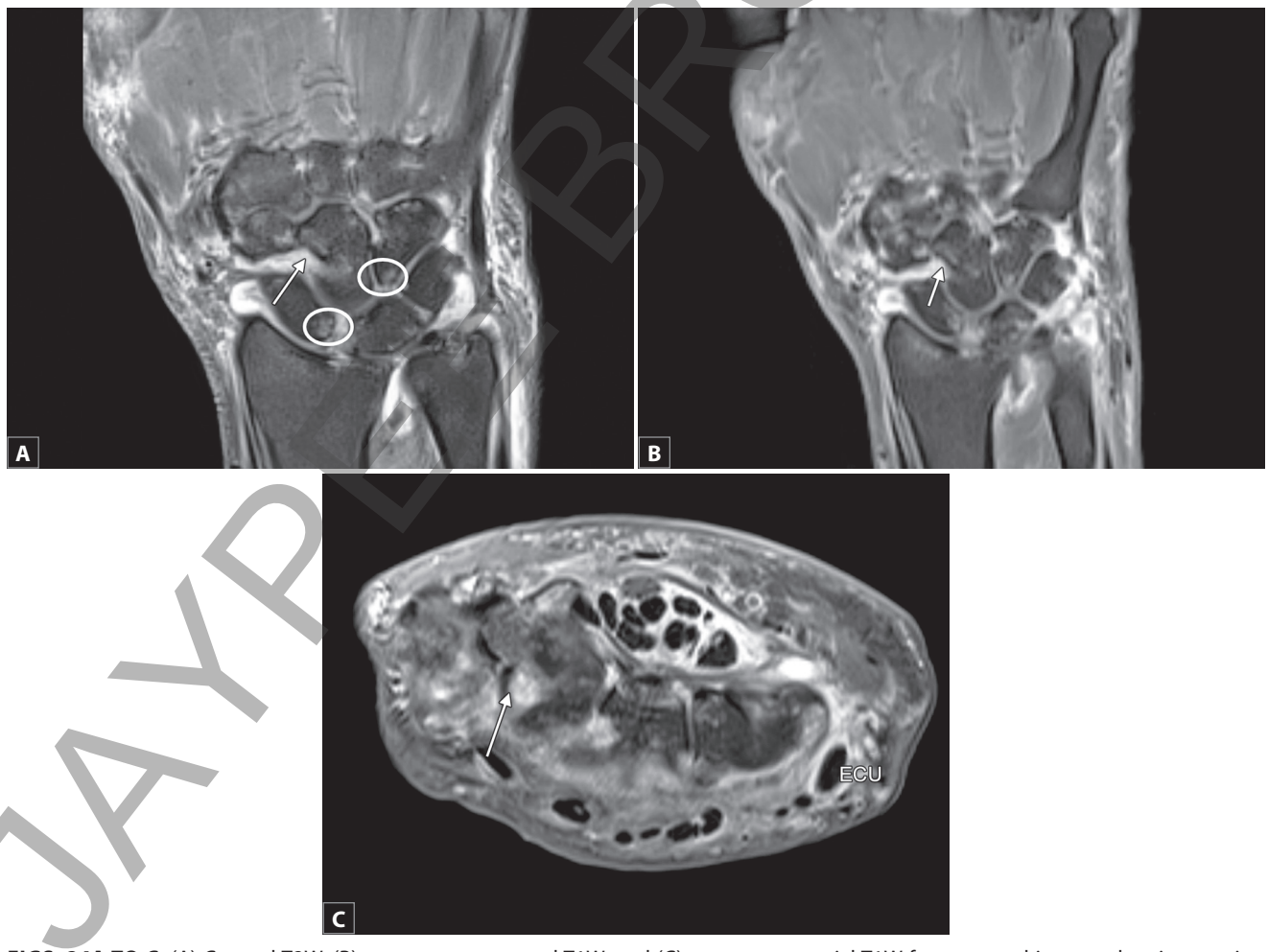
Seronegative Spondyloarthropathies

Magnetic resonance imaging is sensitive in diagnosing erosions, edema, and synovitis but not specific. Similar findings can be detected in other causes of inflammatory arthritis including seronegative spondyloarthropathies such as psoriatic arthritis and Reiter's disease. Involvement of the axial skeleton and enthesitis helps in differentiating between RA and seronegative arthropathies.[57]

Infections

Infectious Tenosynovitis

Acute suppurative tenosynovitis is bacterial and commonly spreads from the adjacent soft-tissue infections after a penetrating injury. Fluid or pus within the tendon



FIGS. 24A TO C: (A) Coronal T2W, (B) postcontrast coronal T1W, and (C) postcontrast axial T1W fat-saturated images showing erosion in capitate (long arrow) and bone marrow edema (oval) in the carpal bones. Synovitis is seen in the distal radioulnar, radiocarpal, ulnocarpal, and intercarpal joints along with tenosynovitis of flexor tendons and extensor carpi ulnaris (ECU). Erosions must be seen in two planes.

JAYPEE BROTHERS

for detailed information on radiology books, visit our website www.ejaypee.com, for detailed information on radiology books, visit our website www.ejaypee.com, for detailed informa



AIIMS-MAMC-PGI IMAGING SERIES

DIAGNOSTIC RADIOLOGY

Musculoskeletal and Breast Imaging

Three decades ago, in 1996, the Departments of Radiodiagnosis of three of India's premier medical institutions—All India Institute of Medical Sciences (AIIMS), New Delhi; Maulana Azad Medical College (MAMC), New Delhi; and Postgraduate Institute of Medical Education and Research (PGIMER), Chandigarh came together with a shared vision: to create a high-quality academic platform for learning and advancing radiology. This collaboration gave rise to the AIIMS-MAMC-PGI Teaching Course Series, which has since grown into a distinguished and enduring academic tradition.

The inaugural course series concluded in 2000, followed by three further editions in 2005, 2013, and 2020, respectively. The sustained enthusiasm of postgraduate students, residents, practicing radiologists, and clinicians has carried this initiative forward to its *5th course series, reaffirming* its place as a unique collaboration among the three institutions.

Each edition focuses on a selected subspecialty of imaging and intervention, bringing together the collective expertise of faculty from these institutions. The accompanying textbook is an integral part of this endeavor, translating the knowledge shared during the course into a lasting reference for clinical practice and postgraduate learning.

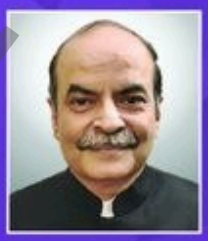
This edition, devoted to *Musculoskeletal and Breast Imaging*, reflects the remarkable evolution of these fields. Comprising 34 chapters, it brings together contemporary concepts, recent advances, updated guidelines and recommendations, and evolving technical developments in diagnostic imaging and image-guided interventions. Particular emphasis has been placed on practical interpretation, relevant anatomy, and optimization of imaging techniques, providing a structured and accessible approach to complex topics.

We hope this book will serve as a valuable companion for *postgraduate students, residents, radiologists,* and *clinicians*, while also providing a practical and up-to-date reference for everyday clinical practice.

"Three institutions. Three decades. One continuing commitment to excellence in radiology."



Akshay Kumar Saxena



Raju Sharma



Alpana Manchanda

JAYPEE BROTHERS

Shelving Recommendation
RADIOLOGY

ISBN 978-81-6799-968-9

9 788167 999689

Buy from ejaypee

JAYPEE BROTHERS